HHS Public Access

Author manuscript

Cell Host Microbe. Author manuscript; available in PMC 2024 September 13.

Published in final edited form as:

Cell Host Microbe. 2023 September 13; 31(9): 1450–1468.e8. doi:10.1016/j.chom.2023.08.002.

Antimicrobial overproduction sustains intestinal inflammation by inhibiting *Enterococcus* colonization

Kyung Ku Jang[1], **Thomas Heaney**[1], **Mariya London**[1], **Yi Ding**[2], **Gregory Putzel**[1,3], **Frank Yeung**[1], **Defne Ercelen**[1], **Ying-Han Chen**[1], **Jordan Axelrad**[4], **Sakteesh Gurunathan**[4], **Chaoting Zhou**[5,6], **Magdalena Podkowik**[3,7], **Natalia Arguelles**[1,3], **Anusha Srivastava**[1,3], **Bo Shopsin**[1,3,7], **Victor J. Torres**[1,3], **A. Marijke Keestra-Gounder**[8], **Alejandro Pironti**[1,3], **Matthew E. Griffin**[9,#], **Howard C. Hang**[9,10], **Ken Cadwell**[6,11,12,13,*]

[1]Department of Microbiology, New York University Grossman School of Medicine, New York, NY 10016, USA

[2]Department of Laboratory Medicine, Geisinger Health, Danville, PA 17822, USA

[3]Antimicrobial-Resistant Pathogens Program, New York University Grossman School of Medicine, New York, NY 10016, USA

[4]Division of Gastroenterology and Hepatology, Department of Medicine, New York University Grossman School of Medicine, New York, NY 10016, USA

[5]Cell and Molecular Biology Graduate Program, Perelman School of Medicine, University of Pennsylvania, Philadelphia, PA 19104, USA

[6]Division of Gastroenterology and Hepatology, Department of Medicine, University of Pennsylvania Perelman School of Medicine, Philadelphia, PA 19104, USA

[7]Division of Infectious Diseases and Immunology, Department of Medicine, New York University Grossman School of Medicine, New York, NY 10016, USA

[*]Correspondence: Ken.Cadwell@Pennmedicine.upenn.edu (K.C.).

[#]Present address: Department of Chemistry, University of California, Irvine, Irvine, CA 92617, USA

AUTHOR CONTRIBUTIONS

K.K.J. and K.C. conceived the study and designed the experiments. K.K.J. contributed to all experiments and data analysis. T.H., M.L., and Y.C. helped perform mouse experiments. Y.D. performed histopathology analysis. G.P. and A.P. performed genetic analysis of *Enterococcus* isolates. F.Y. generated *Nod2 Q675W* mice. D.E. performed 16S rRNA sequencing analysis. J.A. and S.G. assisted with the design, analysis, and interpretation of clinical data. C.Z., M. P., N.A., A.S., B.S., and V.J.T. provided technical assistance and resources for sequencing *Enterococcus* isolates. M.E.G. and H.C.H. provided *Lls* and *Efm* strains and associated technical assistance. A.M.K-G. provided *NOD2*$^{fl/fl}$ mice. K.C. oversaw analysis and interpretation of all experiments. K.K.J., Y. D., G.P., and K.C. wrote the manuscript, and all authors commented on the manuscript, data, and conclusion.

Declaration of interests

K.C. has received research support from Pfizer, Takeda, Pacific Biosciences, Genentech, and Abbvie. K.C. has consulted for or received an honoraria from Puretech Health, Genentech, and Abbvie. K.C. is an inventor on U.S. patent 10,722,600 and provisional patent 62/935,035 and 63/157,225. H.C.H. has received research support from Rise Therapeutics and LISCure Biosciences. U.S. patents PCT/US16/28836 (H.C.H.) and PCT/US2020/019038 (H.C.H. and M.E.G.) were obtained for the commercial use of SagA-engineered bacteria. Rise Therapeutics has licensed these patents to develop SagA-probiotics as therapeutics. J.A. reports consultancy fees, honoraria, or advisory board fees from Abbvie, Adiso, Bristol Myers Squibb, Janssen, Pfizer, Fresnius, and BioFire Diagnostics.

[8]Department of Immunology and Microbiology, University of Colorado School of Medicine, Anschutz Medical Campus, Aurora, CO 80045, USA

[9]Department of Immunology and Microbiology and Department of Chemistry, Scripps Research, 10550 North Torrey Pines Road, La Jolla, CA 92037, USA

[10]Department of Chemistry, Scripps Research, 10550 North Torrey Pines Road, La Jolla, CA 92037, USA

[11]Department of Systems Pharmacology and Translational Therapeutics, University of Pennsylvania Perelman School of Medicine, Philadelphia, PA 19104, USA

[12]Department of Pathology and Laboratory Medicine, University of Pennsylvania Perelman School of Medicine, Philadelphia, PA 19104, USA

[13]Lead Contact

SUMMARY

Loss of antimicrobial proteins such as REG3 family members compromises the integrity of the intestinal barrier. Here, we demonstrate that overproduction of REG3 proteins can also be detrimental by reducing a protective species in the microbiota. Patients with inflammatory bowel disease (IBD) experiencing flares displayed heightened levels of secreted REG3 proteins that mediated depletion of *Enterococcus faecium* (*Efm*) from the gut microbiota. *Efm* inoculation of mice ameliorated intestinal inflammation through activation of the innate immune receptor NOD2, which was associated with the bacterial DL-endopeptidase SagA that generates NOD2-stimulating muropeptides. NOD2 activation in myeloid cells induced IL-1β secretion to increase the proportion of IL-22-producing $CD4^+$ T helper cells and innate lymphoid cells that promote tissue repair. Finally, *Efm* was unable to protect mice carrying a *NOD2* gene variant commonly found in IBD patients. Our findings demonstrate that inflammation self-perpetuates by causing aberrant antimicrobial activity that disrupts symbiotic relationships with gut microbes.

eTOC Blurb

Jang et al. demonstrate that antimicrobial REG3 proteins overproduced during inflammatory bowel disease perpetuate inflammation by depleting *Enterococcus faecium* from the microbiota. DL-endopeptidase SagA secreted by *E. faecium* activates myeloid NOD2 signaling to produce IL-1β, which induces the protective cytokine IL-22 from lymphoid cells.

Graphical Abstract:

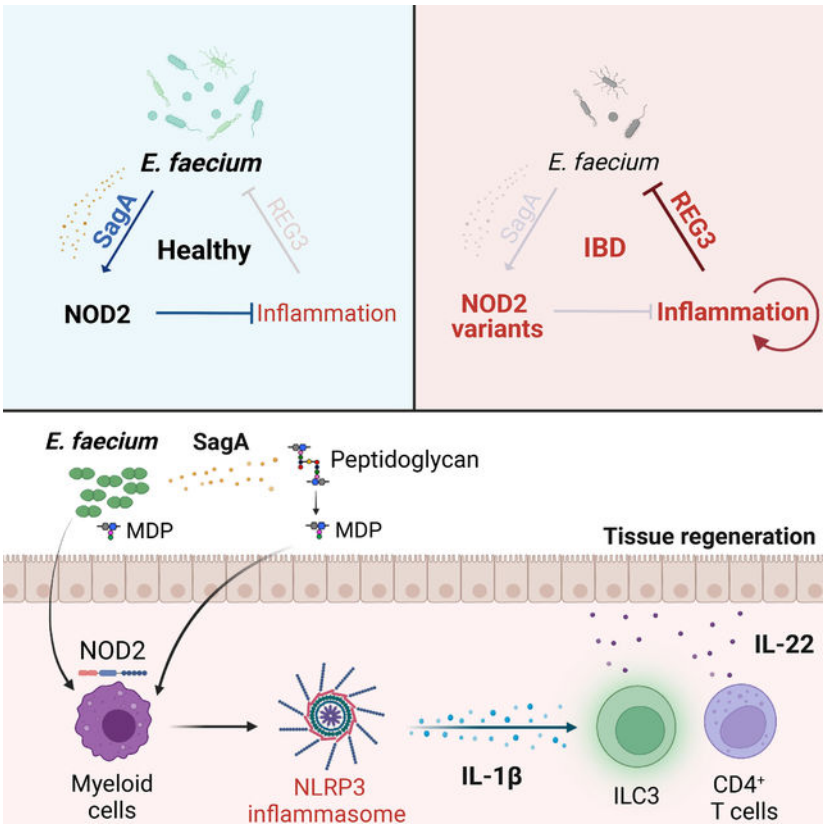

Keywords

Enterococci; antimicrobial proteins; REG3; NOD2; inflammatory bowel disease

INTRODUCTION

Secretion of antimicrobial proteins (AMPs) at barrier surfaces represents a ubiquitous and evolutionarily ancient defense strategy. AMPs such as defensins and C-type lectins are abundant in the mammalian gastrointestinal tract where they limit the overgrowth of microbes, typically by disrupting membrane integrity of their targets[1–3]. Although certain AMPs recognize structures of invasive bacteria such as flagellin[4], many display broad-spectrum activity, reflecting the diversity of pathogenic and non-pathogenic microbes in the gut. Regenerating family member 3 (REG3) C-type lectins REG3A and REG3G bind to the peptidoglycan cell wall of Gram-positive (+) bacteria in the gut[5,6]. *Reg3γ* in mice mediates spatial segregation between the host and the microbiota[7–9]. REG3A (known as HIP/PAP), the main paralog in human, may have a similar role as murine Reg3γ because its transgenic expression in mice alters microbiota composition[10]. Additionally, REG3 proteins regulate intestinal crypt regeneration and scavenge reactive oxygen species[10,11]

Dysregulated AMP production is associated with human inflammatory bowel disease (IBD)[12–17], a chronic immune-mediated disorder of the gut involving complex interactions between genetic and environmental factors. Although immunomodulatory medications can

offer substantial relief to patients, maintaining disease remission remains a major challenge. Consistent with the link between AMPs and intestinal inflammation, an altered microbiota composition is a common feature of IBD[18–20]. Also, population genetic studies have implicated genes associated with host-microbe interactions[21,22]. Variants of the intracellular microbial sensor nucleotide-binding oligomerization domain-containing protein 2 (NOD2) are among the strongest genetic risk factors for IBD[23,24]. NOD2 mediates production of AMPs and cytokines in the presence of peptidoglycan byproducts[23]. *Nod2*-deficient mice are susceptible to enteric bacterial infections and display an altered microbiota composition depending on the animal facility[25–34], and IBD patients harboring *NOD2* variants display impaired production of AMPs[35–37]. However, *NOD2* variants are found in only a subset of IBD patients, indicating that additional mechanisms may be involved. Also, IBD is associated with increased *REG3* expression[38,39], suggesting a different role for these AMPs in disease pathogenesis.

Enterococcus species, Gram+ bacteria in the gut microbiota that activate and are controlled by NOD2[40–42], are highly sensitive to killing by REG3A and REG3G[6,9]. The relationship between enterococci and IBD is debatable. *Enterococcus* species are opportunistic pathogens in hospital settings[43] and induce intestinal inflammation in *Il10*-deficient mice[44,45]. Yet, enterococci are consumed as probiotics for treatment of diarrheal diseases[46,47]. Recent studies identified a DL-endopeptidase, SagA, secreted by certain enterococci including *Enterococcus faecium* (*Efm*)[48–50]. Processing of peptidoglycan by SagA generates muropeptides that activate NOD2 to enhance colonization resistance towards enteric pathogens and antitumor immunity[41,50,51]. Interventions that promote antitumor immunity exacerbate intestinal inflammation[52]. Therefore, it is unclear whether NOD2 activation by enterococci would worsen or improve IBD.

We found IBD patients displayed overproduction of REG3 proteins that deplete enterococci from the gut microbiota. *Efm* or a *Lactococcus* strain engineered to express *sagA* protected mice from intestinal injury through NOD2 activity in myeloid cells, which mediated an increase in lymphoid cells producing the regenerative cytokine IL-22. *Efm* colonization was associated with heightened IL-22 levels in human stool, and this beneficial effect of *Efm* colonization was abrogated in mice harboring the R702W variant of NOD2 associated with IBD. Our findings uncover a mechanism of perpetuating intestinal inflammation initiated by a harmful feedback loop involving excess AMP production and depletion of protective enterococci, which renders the host functionally NOD2-deficient.

RESULTS

REG3 proteins overproduced by IBD patients inhibit enterococci

Although *REG3A* mRNA is increased in inflamed intestinal tissues from IBD patients[38,39], it is unclear whether gene expression is associated with REG3 protein secretion and activity. We collected stool from 56 IBD patients experiencing disease flares (Table S1). An equal number of non-IBD (NIBD) patients experiencing gastrointestinal symptoms, such as diarrhea, were used as a control cohort (Table S2). Stool extracts were used to detect the two human REG3 family members, REG3A and REG3G (Figure 1A), and two additional paralogs: REG1A, a pancreatic growth factor that should not be co-regulated with REG3

proteins[53], and REG4, a less-characterized potential AMP[54,55]. As expected, REG1A was equally present in NIBD and IBD (Figures 1B and 1C). In contrast, REG3A was detected in a higher proportion of IBD patients than NIBD patients, and REG3G and REG4 were exclusively present in IBD samples (Figures 1B and 1C). An ELISA confirmed higher REG3A concentration in stool extracts from IBD than those of NIBD (Figure 1D). Thus, the presence of REG3 proteins is more prevalent and enriched in IBD patients.

We examined the antimicrobial activity of NIBD and IBD stool extracts against *Enterococcus faecalis* (*Efl*) and *Salmonella* Typhimurium (*S*Tm) as Gram+ and − enteric bacteria, respectively. Bacteria displayed modest growth in NIBD stool extracts compared with PBS control, indicating the presence of nutrients in stool (Figure 1E). *Efl* colony forming units (CFUs) after culturing in IBD stool extracts was lower compared with NIBD samples, whereas *S*Tm numbers were similar in both groups (Figure 1E). We confirmed this antimicrobial activity of IBD stool extracts with another *Enterococcus* species, *Efm* (Figure 1E). REG3A concentration negatively correlated with *Efl* and *Efm* CFUs following treatment with NIBD and IBD stool extracts, but not with *S*Tm CFUs (Figure 1F). Additionally, antimicrobial activity against *Efm* in IBD stool extracts was inhibited by antibodies against REG3A or REG3G, individually or together, but not REG1A control antibodies (Figure 1G). Increased numbers of *Efm* were recovered in NIBD stool extracts compared with PBS control, and adding anti-REG3A and REG3G antibodies together enhanced growth, suggesting low levels of antimicrobial activity in these samples (Figure 1G). Thus, *Efm* growth impairment in human stool extracts is attributed to REG3A and REG3G.

IBD stool extracts from both males and females displayed higher amounts of REG3A than NIBD samples (Figure S1A). REG3A concentrations were similar for patients with Crohn's disease (CD) and ulcerative colitis (UC), the two major types of IBD (Figure S1B). REG3A concentration did not differ among age groups in NIBD patients, however, it displayed a modest inverse relationship with age among IBD patients (Figure S1C). We further observed that IBD patients younger than age 60 displayed increased REG3A concentration compared with matched NIBD controls, and this difference was lost in the older age group (Figure S1D). Disease severity displayed a positive correlation with REG3A concentrations (Figure 1H). Thus, REG3A protein overproduction is common to CD and UC flares as described previously for RNA[39].

Enterococcus and *Efm* are lost from the gut microbiota in IBD patients

The above results raise the possibility that *Enterococcus* is depleted in the gut microbiota of IBD patients. 16S rRNA sequencing indicated that the microbiota composition of NIBD and IBD were similar according to alpha and beta diversities (Figures 2A and 2B), confirming that our NIBD cohort is an appropriate control for IBD patients. However, >80% of the sequencing reads aligned to *Enterococcus* for one of the NIBD samples. Thus, we excluded this patient from subsequent analyses. Consistent with our *in vitro* findings (Figure 1), the relative abundance of *Enterococcus* in IBD patients was lower than that in NIBD patients (Figure 2C).

Enterococci are resistant to lysis techniques[56–59]. High-throughput sequencing techniques yield inaccurate measurements of taxa resistant to lysis[60], potentially explaining why prior studies did not observe reduced *Enterococcus* in IBD patients[61–63]. Plating stool on selective agar confirmed our 16S sequencing result and showed that the burden and detection rate of total *Enterococcus* and *Efm* in IBD specimens were lower than in NIBD (Figures 2D and S1E). *Efm*-specific DNA was also detected in stool from NIBD patients more frequently than IBD patients (Figures 2E and 2F). *Efm* accounted for 15% of the total enterococci in IBD compared with 36% in NIBD, indicating that *Efm* was particularly vulnerable to depletion in IBD patients. (Figure S1F). Total *Enterococcus* and *Efm* burden in IBD stool displayed a negative correlation with REG3A concentration (Figure 2G) and with disease severity (Figure 2H).

To increase taxonomical resolution, we sequenced the genomes of 79 and 122 *Enterococcus* isolates collected from 8 NIBD and 11 IBD patients (Table S3). *Efm* represents a higher proportion of the total *Enterococcus* isolates from NIBD stool than IBD stool (Figure S1G). Phylogenetic tree analysis revealed a comparable distribution of *Enterococcus* isolates among NIBD and IBD patients (Figure S1H). Isolates within a species were resolved by grouping into clusters of species variants having less than 100 single nucleotide polymorphisms (SNPs) different from each other (Figure S1I). NIBD patients displayed a higher number of *Enterococcus* variants than IBD patients (Figures S1J and S1K). Half of NIBD patients possessed more than 3 different *Enterococcus* variants whereas less than 2 variants were detected in most IBD patients (Figure S1K). These results are consistent with a loss of diversity of enterococci due to a bottleneck imposed by the increased REG3 proteins in IBD patients.

Enterococci protect against intestinal injury in mice through NOD2

We next examined the relationship between *Enterococcus* and intestinal inflammation. While optimizing conditions for administering dextran sulfate sodium (DSS) in drinking water, a model of intestinal chemical injury, we observed extreme differences in susceptibility between wild-type (WT) C57BL/6J (B6) mice bred in two rooms within the same vivarium. Mice bred in room 6 (Rm 6) receiving 5% DSS displayed higher lethality, weight loss, and disease score compared with mice raised in room 13 (Rm 13) (Figures 3A–3C). Lipocalin-2 (LCN2), a marker of inflammation[64], was more abundant in stool from DSS-treated Rm 6 mice compared with Rm 13 mice (Figure 3D). Shortening of the colon, another marker of intestinal inflammation, was more pronounced in Rm 6 than Rm 13 mice on day 9 (Figure 3E). Susceptibility to DSS diverges due to differences in microbiota composition that arise from separate parental lineages[65,66]. Because we were investigating enterococci, we examined their presence in the microbiota and observed a 2-log higher burden of endogenous enterococci in Rm 13 mice than Rm 6 mice (Figure 3F). Similar to the human samples, *Enterococcus* levels decreased following DSS-induced intestinal inflammation in mice (Figure 3G). In all subsequent experiments, we used mice from Rm 6.

To determine whether *Enterococcus* colonization protects against intestinal injury, we inoculated mice by administering *Efm* in the drinking water[67] and then switched to 5% DSS. Body weight and fecal LCN2 were unchanged in *Efm*-colonized mice without DSS

treatment (Figures S2A and S2B). In mice receiving DSS, both total *Enterococcus* and *Efm* levels decreased during the treatment and partially recovered after cessation (Figures S2C and S2D). Although it is unclear whether REG3 proteins in mice and humans are equivalent in their function[68,69], they both impact *Enterococcus* colonization. The expression of *Reg3α*, *Reg3β*, *Reg3γ*, *Reg3δ*, and *Reg4* reached the peak on day 20 and then gradually decreased, and their expression was inversely associated with both total *Enterococcus* and *Efm* burden (Figures S2E–S2G).

Efm-colonized WT B6 mice treated with DSS displayed less body weight reduction, disease score, and fecal LCN2 compared with DSS-treated mice that did not receive *Efm* (Figures 3H, 3I, S2H, and S2I). On day 23, *Efm*-colonized mice displayed less colon shortening and histopathologic changes (Figures 3J–3L; see Table S4). Inoculating mice with *Efm* after DSS treatment also mitigated these signs of disease (Figures S3A–S3G; see Table S4). To link the *Efm*-mediated protection in mice with our findings in human specimens, we inoculated mice with 3 *Efm* isolates from NIBD patients (Table S3) and confirmed colonization (Figure S2J). Mice colonized with any of the 3 isolates displayed less body weight reduction and colon shortening than those that were untreated (Figures 3M, 3N, and S2K). Therefore, *Efm* confers protection against DSS-induced inflammation.

Given that *Efm* protects against enteric pathogens in a NOD2-dependent manner[41], *Efm* should lose its beneficial properties in *Nod2*-deficient mice during intestinal injury. The colonization patterns of *Efm* in $Nod2^{+/-}$ and $Nod2^{-/-}$ mice were consistent with those in WT mice (Figure S2L). In contrast to $Nod2^{+/-}$ mice in which we reproduced the protective effect of the bacterium, *Efm* administration to $Nod2^{-/-}$ mice did not ameliorate signs of disease (Figures 3O–3S, S2M, and S2N; see Table S4). Lastly, we inoculated $Nod2^{+/-}$ and $Nod2^{-/-}$ mice with *Enterococcus* strains collected from Rm 6 or Rm 13 mice and confirmed they achieved a similar degree of colonization (Figure S2O). Rm 13 *Enterococcus*, but not Rm 6 *Enterococcus*, protected $Nod2^{+/-}$ mice from weight reduction, disease score, and colon shortening following DSS treatment, whereas $Nod2^{-/-}$ mice remained susceptible with either source of *Enterococcus* (Figures 3T, 3U and S2P). Thus, certain *Enterococcus* species including *Efm* confer protection against intestinal injury in a *Nod2*-dependent manner.

SagA mediates NOD2-dependent protection against intestinal injury

SagA secreted by *Efm* generates NOD2-stimulating muropeptides[41,50]. Because SagA is essential for growth of *Efm*[70], we tested the role of SagA by orally inoculating mice with *Lactococcus lactis* (*Lls*) expressing wild-type SagA ($Lls\text{-}sagA^{WT}$) or catalytically inactive (C443A) SagA ($Lls\text{-}sagA^{C443A}$) (Figure S4A). A lower concentration of DSS (3%) was used because mice were pre-treated with antibiotics (abx) to facilitate *Lls* colonization, and abx increases susceptibility to DSS[71,72]. Inoculation with PBS and the parental *Lls* strain were used as controls for effects of abx treatment and *Lls* colonization, respectively. *Lls* strains displayed a similar degree of colonization (Figures S4B and S4D). Mice given $Lls\text{-}sagA^{WT}$ displayed enhanced survival compared with all the other conditions, and other disease parameters were generally improved (Figures 4A–4E and S4C). $Lls\text{-}sagA^{WT}$ ameliorated disease in $Nod2^{+/-}$ mice but not $Nod2^{-/-}$ mice (Figures 4F–4J and S4E). If protection is mediated through peptidoglycan processing by secreted SagA, bacterial colonization would

potentially be dispensable. To test this, we administered filtered culture supernatants from *Lls* strains to mice without abx treatment and then switched to 5% DSS (Figure S4F). In contrast to supernatant from the parental *Lls* and *Lls-sagA*^{C443A} cultures, or sterile broth, supernatant from *Lls-sagA*^{WT} was sufficient for reducing mortality, weight loss, disease score, fecal LCN2, and colon shortening (Figures 4K–4M, S4G, and S4H). These protective effects of *Lls-sagA*^{WT} culture supernatant were NOD2-dependent (Figures 4N–4P, S4I, and S4J). These findings indicate that activating NOD2 downstream of SagA protects against intestinal injury.

The decreased *Efm* burden in IBD patients suggests that SagA-mediated NOD2 activation would be reduced in these individuals. Indeed, SagA was detected in NIBD specimens at both a higher frequency and levels compared with IBD (Figures 4Q–4S). Also, SagA levels negatively correlated with REG3A concentration in IBD patients (Figure 4T). We found higher NOD2 activity using reporter cells stimulated with NIBD stool extracts than IBD samples (Figure 4U). Therefore, the decrease in *Efm* observed in IBD is associated with reduced availability of NOD2 ligands.

NOD2 in myeloid cells is indispensable for *Efm*-mediated protection

NOD2 has been extensively investigated in myeloid and intestinal epithelial cells[73–75]. Therefore, we developed *Nod2*$^{fl/fl}$*;LysM-Cre* and *Villin-Cre* mice that are *Nod2*-deficient in myeloid and intestinal epithelial cells, respectively, and confirmed the presence of *Efm* in stool following inoculation (Figures 5A and 5G). Unlike *Nod2*$^{fl/fl}$ controls in which signs of disease were ameliorated, *Efm* colonization of *Nod2*$^{fl/fl}$*;LysM-Cre*$^{+}$ mice did not improve disease parameters (Figures 5B–5F). In contrast, *Efm* reduced mortality, body weight reduction, disease score, fecal LCN2, and colon length in *Nod2*$^{fl/fl}$*;Villin-Cre*$^{+}$ mice to a similar extent as *Nod2*$^{fl/fl}$ controls (Figures 5H–5L). Thus, NOD2 is required in myeloid cells and dispensable in the intestinal epithelium for *Efm*-mediated protection.

Efm induces IL-22 production by lymphoid cells downstream of myeloid NOD2

NOD2 activation in myeloid cells is frequently associated with pro-inflammatory cytokine production[73–75]. One way to reconcile this established function with our observations would be if NOD2-activated myeloid cells act on other cell types to produce factors involved in tissue repair such as the cytokine IL-22, which is protective in DSS models[76,77]. We observed increased IL-22 production in gut explants harvested from WT mice on day 14 following *Efm* administration (prior to DSS) and day 20 (with DSS) compared with uncolonized mice (Figures 6A and 6B). IL-22 secretion was not enhanced by *Efm* in *Nod2*$^{-/-}$ and *Nod2*$^{fl/fl}$*;LysM-Cre*$^{+}$ mice on days 14 and 20 (Figures 6A and 6B). Group 3 innate lymphoid cells (ILC3s) and CD4^{+} T cells produce IL-22 in the gut. *Efm* increased the proportion and number of both IL-22^{+} ILCs and CD4^{+} T cells in WT mice, and not *Nod2*$^{-/-}$ and *Nod2*$^{fl/fl}$*;LysM-Cre*$^{+}$ mice (Figures 6C–6F, S5A–S5D). NOD2 in antigen-presenting cells can induce IL-10 production from regulatory T cells (Tregs)[78]. However, *Efm* did not alter the proportion of IL10^{+} CD4^{+} T cells, CD4^{+} T helper 1 (Tbet^{+}) and 2 (GATA3^{+}) cells, and Tregs (Figures S5F–S5I). Consistent with ILC3s being a source of IL-22, *Efm* increased the proportion and number of ILC3s and not the proportion of ILC1s and ILC2s in a NOD2-

dependent manner (Figure 6G, 6H, S5E, S5J, and S5K). Therefore, *Efm* induces expansion of IL-22-producing $CD4^+$ T cells and ILCs in a myeloid NOD2-dependent manner.

IL-1β from intestinal myeloid cells induces IL-22 production from ILC3s[79,80]. Also, myeloid-derived IL-1β in response to the microbiota depends on NOD2[81]. The secretion of IL-1β, but not IL-18, was induced in *Efm*-colonized WT, $Nod2^{+/-}$, and $Nod2^{fl/fl}$;*LysM-Cre*$^-$ mice on days 14 and 20 (Figures 6I, 6J, S6A, and S6B). IL-23, another cytokine that induces IL-22 from lymphoid cells[82], was not detected in gut explants. *Efm* did not induce IL-1β in $Nod2^{-/-}$ and $Nod2^{fl/fl}$;*LysM-Cre*$^+$ mice, indicating that *Nod2*-dependent sensing of *Efm* in myeloid cells is required for the upregulated IL-1β secretion (Figures 6J and S6B). Rm 13 mice also displayed increased IL-1β and IL-22 (Figure S6C).

To confirm whether IL-22 is required for *Efm*-mediated protection, we generated $Il22ra1^{fl/fl}$;*Villin-Cre* mice in which IL-22 receptor subunit α is deficient in intestinal epithelial cells and confirmed the *Efm* shedding in stools following inoculation in all groups (Figure 6K). $Il22ra1^{fl/fl}$;*Villin-Cre*$^+$ mice displayed exacerbated intestinal injury compared with $Il22ra1^{fl/fl}$;*Villin-Cre*$^-$ mice, which did not improve with *Efm* colonization (Figures 6L–6O).

Based on these results in mice, we examined the correlation between *Efm* burden and IL-22 production in NIBD and IBD patients. We detected IL-22 protein in NIBD and IBD stool extracts (Figure S6D). Although the detection frequency of IL-22 was comparable between NIBD and IBD, IL-22 intensity was higher in IBD samples (Figures S6E and S6F) as described previously[83]. Among NIBD patients, *Efm* colonization was associated with higher IL-22 levels than the *Efm*-negative patients (Figure S6F). If the heightened IL-22 in IBD patients reflects unresolved inflammation, this relationship would be lost in IBD patients. Indeed, IL-22 levels were comparable between *Efm*-positive and -negative IBD patients (Figure S6F). Among *Efm*-positive individuals, we observed a correlation between IL-22 and *Efm* burden in NIBD patients, which was less obvious in IBD patients (Figure S6G), suggesting a conserved association between *Efm* colonization and IL-22 production in mice and humans.

Efm directly induces IL-1β upstream of IL-22

Efm may act through other microbiota members. However, alpha and beta diversities of the gut microbiota were similar when comparing 16S rRNA sequencing of stool from mice ± *Efm* colonization (Figures S6H and S6I). Analysis of composition of microbiomes (ANCOM) revealed that *Enterococcus* and *Stenotrophomonas* were the only two taxa significantly altered by *Efm* colonization (Figures S6J and S6K). Of note, endogenous *Enterococcus* was undetectable by sequencing, but readily detected by the culture-based method (Figure S6L). Given that *Efm* colonization marginally changes in the microbiota composition, we tested whether *Efm* would be sufficient for promoting the IL-22 response. Introducing *Efm* into germ-free (GF) mice led to stable colonization without changes in body weight and colon length (Figures S6M–S6O). IL-1β and IL-22 were increased in *Efm*-monocolonized mice compared with GF control mice while IL-18 was comparable (Figure S6P).

To confirm whether IL-1β is required for IL-22 production, we quantified these cytokines in gut explants from IL-1 receptor-deficient mice. Although *Efm* promoted IL-1β secretion in both *Il1r1*$^{+/-}$ and *Il1r1*$^{-/-}$ mice, IL-22 was not induced in *Il1r1*$^{-/-}$ mice (Figure S6Q). IL-1β can be produced following its transcription (priming) and post-translational activation by the NLRP3 inflammasome[84,85]. Consistent with a role for NOD2 in priming[86], *Efm* induced *Il1β* and *Nlrp3* expression (Figure S6R). *Il18* transcript and IL-18 secretion were not affected by *Efm*, possibly due to NLRP3-independent regulation of IL-18 in the gut[87,88]. *Efm* increased secretion of IL-1β and IL-22 in *Nlrp3*$^{+/-}$ mice but not in *Nlrp3*$^{-/-}$ mice (Figure S6S). Thus, inflammasome priming by *Efm* induces *Il1β* expression to promote IL-22 production.

NOD2 R702W equivalent impairs *Efm*-mediated protection in mice

The three major NOD2 variants linked to IBD – R702W, G908R, and a frameshift deletion mutation at L1007 (L1007fs) – result in the loss of muropeptide recognition and NF-κB signaling *in vitro*[89,90]. Mice harboring a frameshift mutation equivalent to L1007fs display a compromised cytokine response during bloodstream infection by *Efi*[42], confirming that it results in loss-of-function. The most common variant R702W is detected in up to 5% of individuals of European descent (Figure S7A) has not been studied using an *in vivo* model (Figure 7A). Thus, we generated mice harboring the equivalent of the human R702W variant (Q675W, Figure S7B). We confirmed the absence of other mutations in *Nod2,* and that NOD2 Q675W protein was produced (Figures S7C and S7D). *Efm* was detected in stool collected from *Nod2*$^{Q675W/+}$ (littermate controls) and *Nod2*$^{Q675W/Q675W}$ mice following administration (Figure S7E). *Nod2*$^{Q675W/+}$ and *Nod2*$^{Q675W/Q675W}$ mice displayed modest mortality, weight loss, or disease score following DSS treatment without *Efm* (Figures 7B–7D), partly due to the high levels of endogenous *Enterococcus* colonization compared with the other mice raised in Rm 6 (Figure S7G). *Efm* did not improve disease parameters in *Nod2*$^{Q675W/Q675W}$ mice, and as such, *Efm* colonized mice were more susceptible to DSS than similarly treated *Nod2*$^{Q675W/+}$ mice (Figures 7B–7H, and S7F;see Table S4). Also, IL-1β and IL-22 were not induced by *Efm* in *Nod2*$^{Q675W/Q675W}$ mice (Figure 7I). Thus, the NOD2 R702W equivalent in mice impairs *Efm*-mediated protection.

DISCUSSION

Previous studies demonstrated excessive *REG3* gene expression in IBD despite that AMP secretion is generally associated with an improved mucosal barrier[39]. Here, we revisited this counterintuitive observation. We showed increased REG3 antimicrobial activity in IBD patients compared with controls matched for gastrointestinal symptoms, indicating that REG3 overproduction is specific to IBD flares. Because enterococci are among the most sensitive bacteria to REG3-mediated killing[6,9], we focused our analysis on this group and showed their reduced presence and diversity in IBD patients. Our results in mice show that SagA-secreting enterococci such as *Efm* activate NOD2 in myeloid cells to induce IL-1β, leading to an increase in lymphoid cell types that produce the protective cytokine IL-22. Our findings in humans further support this mechanism by showing that IL-22 levels were associated with *Efm* colonization in NIBD patients, who display heightened NOD2 activity compared with IBD patients. Once the inflammation has been resolved in a non-IBD setting,

enhanced IL-22 may maintain optimal REG3 expressions through STAT3 activation[91], perpetuating gut homeostasis. In IBD, either depletion of NOD2 ligand due to REG3 overproduction or genetic deficiency in NOD2 function disrupts this anti-inflammatory circuit (Figure S7H). This model helps explain how IBD patients with intact NOD2 can develop disease presentations similar to those observed in individuals with NOD2 variants once inflammation is established.

Our study also reveals how endogenous *Enterococcus* in the mouse microbiota can influence experimental outcomes. WT B6 mice maintained in separate rooms displayed substantial differences in susceptibility to DSS due to differences in endogenous *Enterococcus* burden. Also, untreated *Nod2*$^{+/-}$ and *Nod2*$^{-/-}$ mice displayed 4-logs lower *Enterococcus* burden than with *Efm* inoculation (Figures S2C and S2D), and hence comparable susceptibility to intestinal injury. Additionally, not all enterococci are protective. *Enterococcus* isolated from mice resistant to intestinal injury (Rm 13) better-protected recipient mice compared with *Enterococcus* isolated from mice susceptible to DSS (Rm 6) (Figures 3T, 3U, and S2P). Therefore, it may be necessary to monitor *Enterococcus* colonization carefully in studies that examine NOD2 function.

Observations with mice deficient in *Reg3γ* or expressing human *REG3A* in hepatocytes indicate these AMPs suppress intestinal inflammation[10,92]. Although we cannot rule out differences in how these proteins are regulated in mice versus humans, these observations could be explained by a model in which REG3 proteins are protective during homeostasis and harmful during chronic inflammation. Altered availability of oxygen and nitrate in the inflamed gut favors colonization by facultative anaerobic *Enterobacteriaceae* species over the strictly anaerobic *Firmicutes*, the phylum that includes enterococci[93,94]. Other *Firmicutes* reduced in IBD patients encode DL-endopeptidases, such as *Streptococcus cristatus*, *Lactobacillus rhamnosus*, and *Bacteroides caccae*[40]. AMP dysregulation could exacerbate depletion of NOD2-activating species already vulnerable due to imbalanced redox status of the inflamed environment. REG3 overproduction may explain why individuals experiencing transient gastroenteritis recover while IBD patients remain susceptible to disease flare.

Our findings have relevance to other disease settings such as cancer. Probiotics engineered to secrete SagA were shown to improve the efficacy of immune checkpoint blockade therapy in reducing tumors in mice[50]. Although adverse events such as colitis hinder cancer immunotherapy strategies, our results predict that inducing NOD2 through SagA would promote checkpoint inhibitor efficacy while also reducing intestinal inflammation. However, our findings with the *Nod2 Q675W* knock-in mice suggest that this approach will fail in individuals homozygous for analogous loss-of-function variants of NOD2. Genetic information may be useful for matching patients with optimal microbiota-targeting therapies. Additionally, administration of live bacteria is associated with substantial safety concerns. In this context, it is notable that we achieved a similar degree of protection against intestinal injury by administering sterile supernatant collected from SagA-producing bacterial cultures. Postbiotic strategies using bacterial products may be a safe alternate to beneficially trigger NOD2.

Limitations of the study

The consequence of *Enterococcus* depletion on intestinal inflammation and the immune mechanism was investigated in an animal model. A long-term goal would be to test the efficacy and safety of therapies based on this mechanism. For instance, IL-1β production promotes intestinal inflammation in the IL-10-deficient setting[95]. Also, our proposed immune circuit induced by NOD2 in myeloid cells is not mutually exclusive with the multitude of other ways in which NOD2 can protect the intestinal barrier.

STAR METHODS

RESOURCE AVAILABILITY

Lead contact—Further information and requests for resources and reagents should be directed to and will be fulfilled by the Lead Contact, Ken Cadwell (Ken.Cadwell@Pennmedicine.upenn.edu).

Materials availability—The materials in the current study are available from the Lead Contact with a completed Materials Transfer Agreement.

Data and code availability

- 16S rRNA sequencing and whole genome sequencing data are deposited in the NCBI Sequence Read Archive (SRA) and are publicly available as of the date of publication. Accession numbers for the datasets are listed in the key resources table.
- This study does not report original codes.
- Any additional information required to reanalyze the data reported from the Lead Contact upon request.

EXPERIENTAL MODEL AND STUDY PARTICIPANT DETAILS

Mice—Age- and gender-matched 7 to 10-week-old mice on the C57BL/6J (B6) background were used. All mice were bred on-site. Mice harboring gene deletions were compared to their respective littermate control mice indicated in the results section. *Nod2*$^{-/-}$, *LysM-Cre*, *Villin-Cre*, *Il1r1*, and *Nlrp3* mice were purchased from The Jackson Laboratory. *Il22ra1*$^{fl/fl}$ and *Nod2*$^{fl/fl}$ mice were obtained from Sergei Koralov (New York University Grossman School of Medicine) and A. Marijke Keestra-Gounder (University of Colorado Anschutz School of Medicine)[96], respectively. To generate cell type-specific knock-out mice, *Nod2*$^{fl/fl}$ mice were bred with *LysM-Cre* and *Villlin-Cre* mice and *Il22ra1*$^{fl/fl}$ mice were bred with *Villin-Cre* mice. Mice were assigned numbers to facilitate blind data collection and distributed randomly to treatment groups. All animal studies were performed according to approved protocols by the NYU Grossman School of Medicine Animal Care and Use Committee (IACUCs).

Generation of *Nod2 Q675W* knock-in mice—CRISPR–Cas9 gene-targeting mixture containing sgRNA (5’-AGCGGGCACGTGCCTGACGC-3’) targeting exon 4 of B6 *Nod2* and template (5’-

TCACAGCAGCCTTCCTAGCAGGTCTGTTGTCCCAGCAGCATCGGGACCTGTTGGC TGCATGCCAGGTCTCCGAGAGGGTACTTCTATGGCGTCAGGCACGTGCCCGCTCG TGTCTGGCCCACAGCCT-3') (synthesized at Integrated DNA Technologies) and Cas9 mRNA were injected into the cytoplasm of zygotes generated from B6 females impregnated by B6 males, and then the microinjected embryos were incubated in potassium-supplemented simplex optimized medium (KSOM) at 37°C for one day and subsequently transferred into pseudopregnant CD-1 female mice at the two-cell stage by the Rodent Genetic Engineering Laboratory at NYU Grossman School of Medicine. The resulting F0 chimeras were screened through genotyping PCR. Amplicons were generated using a pair of primers (Fwd 5'-CTTTTCAGCTGTGGCCGGCT-3' and Rev 5'-TTTGCCACAGGCCCAATCGG-3') flanking the targeting sites from tail DNA from chimeras and wild-type mice and cut by BsaHI (NEB) (Figure S7A). A 3042-bp region containing the *Nod2* coding region was sequenced to verify correct gene targeting (Figure S7C). All mice used in experiments were backcrossed with B6 mice at least 3 generations.

Gnotobiotics—Previously described GF mice[97] were maintained in flexible film isolators, and absence of fecal bacteria and fungi was confirmed by aerobic culture in brain heart infusion (BHI) (BD), Sabouraud dextrose (Millipore), and nutrient broth (Millipore) and qPCR for bacterial 16S and eukaryotic 18S ribosomal RNA (rRNA) genes through sampling of stool from individual cages in each isolator on a monthly basis. Mice were transferred into individually ventilated Tecniplast ISOcages for DSS treatment to maintain sterility under positive air pressure.

Cell culture—HEK-Blue Null2 (InvivoGen) and HEK-Blue NOD2 (InvivoGen) were cultured at 37°C in 5% CO_2 in Dulbecco's Modified Eagle's Medium (DMEM, Corning) in the presence of 10% fetal bovine serum (FBS, Peak Serum), 100 IU/ml penicillin and 100 μg/ml streptomycin (Corning), 100 μg/ml normicin (InvivoGen), and appropriate antibiotics (100 μg/ml zeocin (InvivoGen) for HEK-Blue Null2 and 30 μg/ml blastocidin (InvivoGen) and 100 μg/ml zeocin for HEK-Blue NOD2). Cells were maintained at no greater than 70% confluency and subcultured using Trypsin-EDTA (Gibco). Cell lines were routinely cultured without antibiotics to ensure no bacterial infection and tested for mycoplasma.

Human stool samples and data collection—Stool samples were collected with consent from hospitalized adult non-IBD (NIBD) and IBD patients with gastrointestinal symptoms with consent between June 27, 2019 and February 26, 2020. The protocol has been approved by the New York University School of Medicine Institutional Review Board (Mucosal Immune Profiling in Patients with Inflammatory Bowel Disease; S12–01137). The clinical data of NIBD and IBD patients were collected using EPIC EHR and REDCap 9.3.6 software. A total of 112 patients were included in the analysis, of which 56% were female, median age 44.5. Patient information including age, gender, gastrointestinal symptoms, medical history related with gastrointestinal tract, and disease activity scores (CDAI or total Mayo) are shown in Tables S1 and S2. At the time of sample acquisition and processing, investigators were blinded to the patient clinical status.

METHOD DETAILS

Bacterial species—*Enterococcus faecalis* OG1RF (*Efl*), *E. faecium* Com15 (*Efm*), and *Lactococcus lactis thyA* auxotroph (*Lls*) expressing wild-type SagA (*Lls-sagA*^{WT}) and catalytic mutant SagA (*Lls-sagA*^{C443A}) were previously described[50]. *Salmonella* Typhimurium SL1344 (*S*Tm) was provided by Dan Littman (NYU). *Efl* and *Efm* were grown at 37°C under ambient atmosphere in autoclaved antibiotics-free BHI broth. *Lls* strains and *S*Tm were cultured at the above condition in M17 broth (BD) supplemented with 2% (v/v) lactose (Sigma-Aldrich) and 20 μg/ml of thymidine (Sigma-Aldrich) (LM17 broth) and Luria Bertani (LB) broth (NYU Reagent Preparation Core), respectively. Colony forming unit (CFU) of *Efl*, *Efm*, *Lls* strains, and *S*Tm was enumerated on bile esculin azide (BEA) agar (Millipore), HiCrome *Enterococcus faecium* Agar with Selective Supplement (HIMEDIA), M17 agar (BD) supplemented with 2% (v/v) lactose and 20 μg/ml of thymidine (LM17 agar), and LB agar (NYU Reagent Preparation Core), respectively.

Preparation of human stool extract, antimicrobial activity assay, and REG3A measurement—1 g of human stools from NIBD and IBD patients were homogenized in 5 ml of phosphate-buffered saline (PBS, Corning) using TissueRuptor (Qiagen). 0.5–1 ml of human stool slurries were taken for quantification of bacterial burden. The remaining stool slurries were filtered using a 10 ml syringe (BD) with gauze (4MD Medical). Human stool extracts were collected by centrifugation at 15,000 x *g* for 20 min at 4°C and filter-sterilized using a 10 ml syringe with Millex-GS Syringe Filter Unit, 0.22 μm (Millipore).

For quantifying the antimicrobial activity of the human stool extracts, overnight cultures of *Efl*, *Efm*, and *S*Tm were harvested, resuspended in 50 μl of PBS, and mixed with one volume of human stool extracts or PBS. The mixture of bacteria and human stool extract was incubated in a 37°C static incubator for 24 h and then plated in serial dilution on selective agars as mentioned above for enumerating *Efl*, *Efm*, and *S*Tm.

Quantification of REG3A in human stool extracts was performed using Human Reg3A DuoSet ELISA (R&D systems) according to the manufacturer's instructions.

Western blotting—Mouse colonic tissues were processed for immunoblotting as previously described[97,98]. Briefly, proximal colonic tissues (2 mm) were cut open and washed with PBS, then suspended in lysis buffer (20 mM Tris-HCl (pH 7.4, NYU Reagent Preparation Core), 150 mM NaCl (NYU Reagent Preparation Core), 1% Triton X-100 (Sigma-Aldrich), 10% glycerol (Sigma-Aldrich), and 2x Halt Protease and Phosphatase Inhibitor Cocktail (Thermo Fisher)) and homogenized using FastPrep-24 Classic bead beating grinder and lysis system (MP Biomedicals). Tissue homogenate was then pelleted twice at 10,000 x *g* for 10 min at 4°C to collect the lysates. human stool extracts and mouse colonic tissue lysates were resolved on Bolt 4–12% Bis-Tris Plus Gels (Invitrogen), transferred onto polyvinylidene difluoride membranes, and blocked using Intercept (TBS) blocking buffer (LI-COR). Membranes were probed with primary antibody overnight at 4°C. The following primary antibodies were used for western blotting studies: anti-REG1A (R&D systems, MAB4937), REG3A (R&D systems, MAB5965), REG3G (Abcam, ab233480), REG4 (Abcam, ab255820), SagA[41], IL-22 (R&D systems, MAB782), NOD2

(Invitrogen, MA1–16611), and β-actin (Sigma-Aldrich, A5441). After incubation with the primary antibody, the membrane was washed and probed with the secondary antibody for 1 h at room temperature (RT). As for secondary antibodies, IRDye 680RD Goat anti-Rabbit (925–68071), IRDye 800CW Goat anti-Mouse (925–32210), and IRDye 800CW Goat anti-Rat (925–32219) were purchased from LI-COR. After additional washing, the protein was then detected with Image Studio for Odyssey CLx (LI-COR). Band intensities were measured by Fiji/ImageJ[99]

DNA extraction,16S rRNA sequencing analysis, and detection of *Efm*.—DNA from human stool samples or mouse fecal samples following 2-week-administration of *Efm* in drinking water or control was extracted with DNeasy PowerSoil Pro kit (Qiagen) according to the manufacturer's instruction. Bacterial 16S rRNA gene was amplified at the V4 region using primer pairs and paired-end amplicon sequencing was performed on the Illumina MiSeq system at NYU Genome Technology Core. Sequencing reads were processed using the DADA2 pipeline in the QIIME2 software package. Taxonomic assignment was performed against the Greengenes 13_8 99% OTUs full-length sequences database[100]. Alpha diversity analysis was done using observed OTUs[101]. Beta diversity was calculated using Bray-Curtis, Jaccard, unweighted UniFrac, and weighted UniFrac distance and visualized with EMPeror[102]. Differentially abundant bacterial species were identified by ANCOM[103].

To detect *Efm* from stool DNA of NIBD and IBD patients, 658-bp region specific to genomic DNA of *Efm* was amplified from 25 ng of the stool DNA by PCR using a pair of primers (Fwd 5'-TTGAGGCAGACCAGATTGACG-3' and Rev 5'-TATGACAGCGACTCCGATTCC-3') as described previously[104].

Enumeration of total *Enterococcus* and *Efm* in human stool samples—The human stool slurries (200 mg/ml) were plated in serial dilution on selective agars mentioned above for enumerating CFU of total *Enterococcus* and *Efm*, respectively.

Isolation and genomic analysis of *Enterococcus* strains from NIBD and IBD patients—A total of 201 *Enterococcus* strains were isolated by plating human stool slurries on bile esculin azide agar. The colonies on the plate were further purified by streaking on trypticase soy agar with 5% sheep blood (Henry Schein). Genomic DNA was extracted using the KingFisher Flex automated extraction instrument (Thermo Fisher) and the MagMAX DNA Multi-Sample Ultra 2.0 kit reagents (Applied Biosystems). Genome sequencing was performed on an Illumina NovaSeq 6000 system at the NYU Genome Technology Core, yielding 150 bp paired-end reads. The software fastp v0.20.1[105] was used with default settings to remove adapters, trim low-quality bases, and remove low-quality reads. The level of within-species cross-contamination was estimated using ConFindr[106] version 0.7.4; isolates with predicted contamination greater than 10% were excluded from further analysis. Taxonomic classification to the species level was performed by running GTDBTK[107] version v1.5.1 (database release 202) on genome assemblies generated using Unicycler[108] version v0.4.8 in conservative mode. The presence of *sagA* in each genome assembly was determined using BLAST[109].

Filtered reads from all species were mapped to a reference assembly of *Efm* strain SRR24 (RefSeq accession GCF_009734005.1) using Snippy version 4.6.0 (github.com/tseemann/snippy). A single phylogenetic tree was inferred for all species based on the resulting core alignment using RAxML version 8.2.12[110] using the GTRGAMMA model of evolution.

For each of the *Enterococcus* species identified using GTDBTK, a core alignment of the isolates belonging to that species was generated using Snippy, using one of the isolates' assemblies as reference. A SNP matrix was calculated using snp-dists version 0.8.2 (https://github.com/tseemann/snp-dists). Strains were then defined by clustering isolates using a threshold of 100 SNPs. Specifically, the R package igraph[111] was used to create a graph whose nodes are the isolates and whose edges connect any pair of isolates differing by no more than 100 SNPs in the corresponding within-species alignment. Strains were defined as the connected components of the resulting graph.

Bacterial inoculation and DSS treatment of mice—*Efm* drinking water was prepared as described previously[67]. Briefly, overnight culture of *Efm* was harvested and resuspended in filter-sterilized drinking water to 10^9 CFU/ml, herein referred as *Efm* water, and administered to mice for 14 days. This drinking water was then replaced with one containing 5% dextran sulfate sodium (DSS, TdB Consultancy) for 6 days and then switched to regular drinking water for the remainder of the experiment when examining intestinal injury following *Efm* colonization. For experiments in which *Efm* was administered after the initiation of intestinal injury, mice were treated with 5% DSS for 6 days and received *Efm* water or control water for the remainder of the experiment. Drinking water was exchanged with freshly prepared ones every 2–3 days for all types of treatment.

For *Efm* colonization in GF mice, overnight cultures of *Efm* were harvested and resuspended in PBS to 10^9 CFU/100 μl and were administered to GF mice by oral gavage of 100 μl *Efm* inoculum on day 0. The colonization of *Efm* was confirmed by enumerating CFU in stool pellets on the selective agar plate mentioned above for 2 weeks.

Overnight cultures of *Lls* strains were harvested and resuspended in PBS to 10^9 CFU/100 μl. Water containing ampicillin (1 mg/ml, American Bioanalytical) and streptomycin (0.5 mg/ml, Sigma-Aldrich) was filter-sterilized using Nalgene Rapid-Flow Sterile Disposable Filter Units with PES Membranes (Thermo Fisher) for the antibiotic (abx) treatment. The mice treated with abx-containing water for 7 days were given 3% DSS for 6 days. On days 8 and 14, the mice were orally administered 100 μl inoculum of *Lls* strains (approximately 10^9 CFU).

For treatment of *Lls* culture supernatant, overnight cultures of *Lls* strains were centrifuged at 6,000 x *g* for 15 min at 4°C to collect the culture supernatant. The supernatants and LM17 broth control were filter-sterilized using Nalgene Rapid-Flow Sterile Disposable Filter Units with PES Membranes to avoid bacterial contamination. The mice receiving the filter-sterilized supernatants of *Lls* strains or LM17 broth as drinking water for 7 days were given 5% DSS for 6 days.

For administration of Rm 6 and Rm 13 *Enterococcus*, *Enterococcus* strains were collected by plating stool pellets from Rm 6 or Rm 13 mice on the selective agar plate mentioned above and then harvested for *Enterococcus* drinking water in the same way as *Efm* water preparation. The Rm 6 mice receiving the Rm 6 or Rm 13 *Enterococcus* drinking water for 14 days were given 5% DSS for 6 days.

The mice were monitored daily for survival and weight loss. Disease score was quantified based on five parameters in which eight was the maximum score: diarrhea (0–2), bloody stool (0–1), hunched posture (0–2), mobility (0–2), and fur ruffling (0–1).

Quantification of bacterial burden and lipocalin-2 (LCN2) in murine stool samples—Stool pellets from individual mice were weighed, homogenized in PBS, and plated in serial dilution on selective agars as mentioned above for enumerating CFU of total *Enterococcus*, *Efm*, and *Lls* strains, respectively. The remaining stool homogenates were centrifuged at 15,000 x *g* for 5 min to collect clear supernatants. LCN2 in the clear supernatants was quantified using Mouse Lipocalin-2/NGAL DuoSet ELISA (R&D systems) according to the manufacturer's instructions.

Transcript analysis—Total RNA was extracted from proximal colonic tissue (2 mm) using RNeasy Mini Kit with DNase treatment (QIAGEN), and synthesis of cDNA was conducted with High-Capacity cDNA Reverse Transcription Kit (ThermoFisher) according to the manufacturer's protocol. RT-PCR was performed using SybrGreen (Roche) on a Roch480II Lightcycler using the following primers: *Reg3α*, Fwd 5'-CTCAGGACATCTCGTGTCTATTCTT-3' and Rev 5'-AGTGACCACGGTTGACAGTAGAG-3'; *Reg3β*, Fwd 5'-CTCTCCTGCCTGATGCTCTT-3' and Rev 5'-GTAGGAGCCATAAGCCTGGG-3'; *Reg3γ*, Fwd 5'-CGTGCCTATGGCTCCTATTGCT-3' and Rev 5'-TTCAGCGCCACTGAGCACAGAC-3'; *Reg3δ*, Fwd 5'-TGGAACCACAGACCTGGGCTA-3' and Rev 5'-GAGCAGAAATGCCAGGTGTCC-3'; *Reg4*, Fwd 5'-CGCTGAGATGAACCCCAAG-3' and Rev 5'-TGAGAGGGAAGTGGGAAGAG-3'; *Il18*, Fwd 5'-CAACCAACAAGTGATATTCTCCATG-3' and Rev 5'-CTGACATGGCAGCCATTGT-3'; *Il1β*, Fwd 5'-CAACCAACAAGTGATATTCTCCATG-3' and Rev 5'-GATCCACACTCTCCAGCTGCA-3'; *Nlrp3*, Fwd 5'-CTCCAACCATTCTCTGACCAG-3' and Rev 5'-ACAGATTGAAGTAAGGCCGG-3'; *Gapdh*, Fwd 5'-TGGCCTTCCGTGTTCCTAC-3' and Rev 5'- TGGCCTTCCGTGTTCCTAC-3';. The relative expression of the respective genes to *Gapdh* expression was calculated using the $\Delta\Delta C_T$ method[112] and was expressed as fold change normalized to WT mice before *Efm* Colonization.

Histology—Quantification of colon histology data was performed blind. Colonic tissues were cut open along the length, pinned on black wax, and fixed in 10% formalin (Thermo Fisher). Tissues were embedded in 3% low melting point agar (Promega). Formalin embedding, cutting, and hematoxylin and eosin (H&E) staining were performed by the NYU Histopathology core. Sections were imaged on a Nikon Eclipse Ci microscope. Pathologic changes in colonic mucosa evaluated by Y.D. included colonic epithelium, lamina propria,

muscularis mucosa, and submucosa. It was based on the state of the changes (acute or chronic) and the degree of involvement. Acute changes primarily included neutrophils in the crypt lumen, erosions, ulcers, pus, and the formation of polyps. Features of chronic changes included the following: crypt distortion (sideways crypts, branching, tortuous), crypt loss, crypt atrophy, basal plasmacytosis, and lymphoid aggregates. The involvement pattern included focal distal involvement, patchy involvement with skipping areas, diffuse involvement, and pancolonic (no skip areas) involvement. The percentage of involvement was calculated as 100 x (Length of disease involved colon / Total length of the colon).

NOD2 activity assay—Single-cell suspensions (50,000 cells/ml) of HEK-Blue Null2 or HEK-Blue NOD2 were prepared by tapping the flask and suspension with HEK-Blue detection medium (InvivoGen). Cells were aliquoted at 180 μl/well in a 96-well plate (Corning) containing 20 μl dilutes of human stool extracts in PBS. Cells were then incubated at 37°C in 5% CO_2 for 24 h. To measure activity, wells were then gently pipetted up and down to mix the conditioned medium, and absorbance from the colorimetric product of the secreted alkaline phosphatase was measured at 630 nm. The NOD2 activity was calculated as fold change by normalizing to HEK-Blue Null2 cells.

Colon explant culture and cytokine detection—Colon explant culture was performed as previously described[76]. The proximal colon tissue (1 cm) was opened longitudinally, washed with PBS and cultured for 48 h in 1ml of complete Roswell Park Memorial Institute (RPMI) 1640 (Gibco) containing 2 mM L-glutamine (Corning), 100 IU/ml penicillin and 100 μg/ml streptomycin, 20 mM N-2-hydroxyethylpiperazine-N'-2-ethane sulfonic acid (HEPES, Corning), Minimum Essential Medium (MEM) non-essential amino acids (Corning), 1 mM sodium pyruvate (Corning), and β-mercaptoethanol (Gibco). Cytokines in supernatants were measured using the Mouse IL-22, IL-18, and IL-1 beta/IL-1 F2 DuoSet ELISA (R&D systems) according to the manufacturer's instructions.

Isolation of LP cells—LP cells were harvested as before[113]. Briefly, colonic tissue including caecum was cut open and washed with PBS, and fat was removed. The tissues were incubated with 20 ml of Hank's Balanced Salt Solution (HBSS, Gibco) with 2% HEPES, 1% sodium pyruvate, 5 mM Ethylenediaminetetraacetic acid (EDTA, NYU Reagent Preparation Core), and 1mM DL-dithiothreitol (Sigma-Aldrich) for 15 min at 37°C with 220 rpm and then with new 20 mL of HBSS with 2% HEPES, 1% sodium pyruvate, 5 mM EDTA for 10 min at 37°C with 210 rpm. The tissue bits were washed with HBSS, minced, and then enzymatically digested with collagenase (0.5 mg/ml, Sigma-Aldrich) and Deoxyribonuclease I (0.01 mg/ml, Sigma-Aldrich) for 30 min at 37°C with 200 rpm. Digested solutions were passed through 70 μm nylon mesh (ELKO Filtering) and isolated cells were resuspended in 40% Percoll (Sigma-Aldrich), layered onto 80% Percoll, and centrifuged at RT at 2,200 rpm for 22 min. Cells were recovered from the interphase and washed with RPMI containing 10% FBS (Peak Serum) (cRPMI). For the analysis of the cytokine production, LPLs were plated in cRPMI and stimulated with 1X Cell Stimulation Cocktail (plus transport inhibitors) (eBiosciecne) for 4 h at 37°C.

Flow cytometry—Surface and intracellular cytokine staining was performed per manufacturer's instruction in PBS with 0.5% bovine serum albumin (BSA, Thermo Fisher) (BSA/PBS) for 20 min on ice. Two staining panels were prepared as described previously[113]. The following antibodies were used for the first panel: CD11b (101228, 1:200), CD11c (117328, 1:200), CD127 (135041, 1:33), CD4 (100414, 1:150), CD44 (103030, 1:100), CD62L (104433, 1:100), CD8 (100730, 1:100), GR1 (108428, 1:300), NK1.1 (108736, 1:150), Tbet (644810, 1:50), TCRβ (109243, 1:100), TER119 (116228, 1:200) from Biolegend, CD19 (45–0193-82, 1:100) and FOXP3 (17–5773-82, 1:100) from eBioscience, and CD45 (564279, 1:200), GATA3 (560163, 1:40), RORγt (562894, 1:100), TCRγδ (563532, 1:100) from BD Bioscience. The following antibodies were used for the second panel: CD11b (101228, 1:200), CD11c (117328, 1:200), CD127 (135041, 1:33), CD4 (100414, 1:150), CD8 (100730, 1:100), GR1 (108428, 1:300), NK1.1 (108728, 1:200), TCRβ (109243, 1:100), TER119 (116228, 1:200) from Biolegend, IL-22 (12–7221-82, 1:100) from eBioscience, and CD45 (564279, 1:200), IL-10 (566295, 1:100) and TCRγδ (563532, 1:100) from BD Bioscience. Samples were fixed with either Fixation Buffer (Biolegend) or Foxp3/Transcription Factor Staining Buffer Set (Thermo Fisher). For intracellular staining of the transcription factor, cells were permeabilized with the Foxp3/Transcription Factor Staining Buffer Set at RT for 45 min in the presence of antibodies. For intracellular staining of cytokines, cells were permeabilized with Intracellular Staining Permeabilization Wash Buffer (Biolegend) at RT for 20 min in the presence of antibodies. Zombie UV Fixable Viability Kit (Biolegend) was used to exclude dead cells. Samples were acquired on a BD LSR II (BD Biosciences) and analyzed using FlowJo software (BD).

Nod2* sequencing—Nod2* mRNA was sequenced as previously described [114]. Briefly, total RNA was extracted from proximal colonic tissues (2 mm) and subjected to the synthesis of cDNA using the same kits mentioned above. A 3042-bp region containing the *Nod2* coding region was amplified from cDNA by PCR using a pair of primers (Fwd 5'-ATGTGCTCACAGGAAGAGTTCC-3' and Rev 5'-TCACAACAAGAGTCTGGCGTCCC-3'). Amplicons were cloned into pCR2.1-TOPO (Invitrogen). The plasmids were sequenced by Oxford Nanopore from SNPsaurus.

QUANTIFICATION AND STATISTICAL ANALYSIS

Data points and bars in the figure panels represent mean values ± standard error of mean. Statistical methods in this study are described in the figure legend using GraphPad Prism 9 and Python. N represents individual patient or mouse as described in the figure legend. $p < 0.05$ is considered statistically significant for all assays, and individual p values are indicated in the figure panels.

Supplementary Material

Refer to Web version on PubMed Central for supplementary material.

ACKNOWLEDGEMENT

We would like to acknowledge NYU Grossman School of Medicine Flow Cytometry and Cell Sorting, Microscopy, Genome Technology, Rodent Genetic Engineering, and Histology Cores and Clinical Microbiology Laboratory for use of their instruments and technical assistance (supported by National Institutes of Health [NIH] grants

P31CA016087, S10OD01058, and S10OD018338). This work was supported in part by NIH grants DK093668 (K.C.), AI121244 (K.C.), HL123340 (K.C.), AI130945 (K.C.), AI140754 (K.C.), DK124336 (K.C.), R01AI137336 (B.S.), R01AI140754 (B.S.), AI164154 (A.M.K-G.), AI173121 (A.M.K-G.), DK122698 (F.Y.), and DK132908 (M.L.); Faculty Scholar grant from the Howard Hughes Medical Institute (K.C.), Crohn's & Colitis Foundation (K.C.), Kenneth Rainin Foundation (K.C. and H.C.H.), Bernard Levine Postdoctoral Research Fellowship in Immunology (Y.H.C.), the Charles H. Revson Senior Fellowships in Biomedical Science (Y.H.C.), and NYU Langone Health Antimicrobial-Resistant Pathogens Program (B.S., V.J.T., and A.P.).

Inclusion and diversity

We support inclusive, diverse, and equitable conduct of research.

References

1. Muniz LR, Knosp C, and Yeretssian G (2012). Intestinal antimicrobial peptides during homeostasis, infection, and disease. Front Immunol 3, 310. 10.3389/fimmu.2012.00310. [PubMed: 23087688]
2. Bevins CL, and Salzman NH (2011). Paneth cells, antimicrobial peptides and maintenance of intestinal homeostasis. Nat Rev Microbiol 9, 356–368. 10.1038/nrmicro2546. [PubMed: 21423246]
3. Ramanan D, and Cadwell K (2016). Intrinsic Defense Mechanisms of the Intestinal Epithelium. Cell Host Microbe 19, 434–441. 10.1016/j.chom.2016.03.003. [PubMed: 27049583]
4. Okumura R, Kurakawa T, Nakano T, Kayama H, Kinoshita M, Motooka D, Gotoh K, Kimura T, Kamiyama N, Kusu T, et al. (2016). Lypd8 promotes the segregation of flagellated microbiota and colonic epithelia. Nature 532, 117–121. 10.1038/nature17406. [PubMed: 27027293]
5. Lehotzky RE, Partch CL, Mukherjee S, Cash HL, Goldman WE, Gardner KH, and Hooper LV (2010). Molecular basis for peptidoglycan recognition by a bactericidal lectin. Proc Natl Acad Sci U S A 107, 7722–7727. 10.1073/pnas.0909449107. [PubMed: 20382864]
6. Cash HL, Whitham CV, Behrendt CL, and Hooper LV (2006). Symbiotic bacteria direct expression of an intestinal bactericidal lectin. Science 313, 1126–1130. 10.1126/science.1127119. [PubMed: 16931762]
7. Wang L, Fouts DE, Starkel P, Hartmann P, Chen P, Llorente C, DePew J, Moncera K, Ho SB, Brenner DA, et al. (2016). Intestinal REG3 Lectins Protect against Alcoholic Steatohepatitis by Reducing Mucosa-Associated Microbiota and Preventing Bacterial Translocation. Cell Host Microbe 19, 227–239. 10.1016/j.chom.2016.01.003. [PubMed: 26867181]
8. Vaishnava S, Yamamoto M, Severson KM, Ruhn KA, Yu X, Koren O, Ley R, Wakeland EK, and Hooper LV (2011). The antibacterial lectin RegIIIgamma promotes the spatial segregation of microbiota and host in the intestine. Science 334, 255–258. 10.1126/science.1209791. [PubMed: 21998396]
9. Brandl K, Plitas G, Mihu CN, Ubeda C, Jia T, Fleisher M, Schnabl B, DeMatteo RP, and Pamer EG (2008). Vancomycin-resistant enterococci exploit antibiotic-induced innate immune deficits. Nature 455, 804–807. 10.1038/nature07250. [PubMed: 18724361]
10. Darnaud M, Dos Santos A, Gonzalez P, Augui S, Lacoste C, Desterke C, De Hertogh G, Valentino E, Braun E, Zheng J, et al. (2018). Enteric Delivery of Regenerating Family Member 3 alpha Alters the Intestinal Microbiota and Controls Inflammation in Mice With Colitis. Gastroenterology 154, 1009–1023 e1014. 10.1053/j.gastro.2017.11.003. [PubMed: 29133078]
11. Zhao D, Kim YH, Jeong S, Greenson JK, Chaudhry MS, Hoepting M, Anderson ER, van den Brink MR, Peled JU, Gomes AL, et al. (2018). Survival signal REG3alpha prevents crypt apoptosis to control acute gastrointestinal graft-versus-host disease. J Clin Invest 128, 4970–4979. 10.1172/JCI99261. [PubMed: 30106382]
12. Yu S, Balasubramanian I, Laubitz D, Tong K, Bandyopadhyay S, Lin X, Flores J, Singh R, Liu Y, Macazana C, et al. (2020). Paneth Cell-Derived Lysozyme Defines the Composition of Mucolytic Microbiota and the Inflammatory Tone of the Intestine. Immunity 53, 398–416 e398. 10.1016/j.immuni.2020.07.010. [PubMed: 32814028]
13. Cadwell K, Liu JY, Brown SL, Miyoshi H, Loh J, Lennerz JK, Kishi C, Kc W, Carrero JA, Hunt S, et al. (2008). A key role for autophagy and the autophagy gene Atg16l1 in mouse and human intestinal Paneth cells. Nature 456, 259–263. 10.1038/nature07416. [PubMed: 18849966]

14. Wehkamp J, Salzman NH, Porter E, Nuding S, Weichenthal M, Petras RE, Shen B, Schaeffeler E, Schwab M, Linzmeier R, et al. (2005). Reduced Paneth cell alpha-defensins in ileal Crohn's disease. Proc Natl Acad Sci U S A 102, 18129–18134. 10.1073/pnas.0505256102. [PubMed: 16330776]
15. Koslowski MJ, Kubler I, Chamaillard M, Schaeffeler E, Reinisch W, Wang G, Beisner J, Teml A, Peyrin-Biroulet L, Winter S, et al. (2009). Genetic variants of Wnt transcription factor TCF-4 (TCF7L2) putative promoter region are associated with small intestinal Crohn's disease. PLoS One 4, e4496. 10.1371/journal.pone.0004496. [PubMed: 19221600]
16. Courth LF, Ostaff MJ, Mailander-Sanchez D, Malek NP, Stange EF, and Wehkamp J (2015). Crohn's disease-derived monocytes fail to induce Paneth cell defensins. Proc Natl Acad Sci U S A 112, 14000–14005. 10.1073/pnas.1510084112. [PubMed: 26512113]
17. Bel S, Pendse M, Wang Y, Li Y, Ruhn KA, Hassell B, Leal T, Winter SE, Xavier RJ, and Hooper LV (2017). Paneth cells secrete lysozyme via secretory autophagy during bacterial infection of the intestine. Science 357, 1047–1052. 10.1126/science.aal4677. [PubMed: 28751470]
18. Manichanh C, Borruel N, Casellas F, and Guarner F (2012). The gut microbiota in IBD. Nat Rev Gastroenterol Hepatol 9, 599–608. 10.1038/nrgastro.2012.152. [PubMed: 22907164]
19. Ni J, Wu GD, Albenberg L, and Tomov VT (2017). Gut microbiota and IBD: causation or correlation? Nat Rev Gastroenterol Hepatol 14, 573–584. 10.1038/nrgastro.2017.88. [PubMed: 28743984]
20. Wong SY, and Cadwell K (2018). There was collusion: Microbes in inflammatory bowel disease. PLoS Pathog 14, e1007215. 10.1371/journal.ppat.1007215. [PubMed: 30235350]
21. Jostins L, Ripke S, Weersma RK, Duerr RH, McGovern DP, Hui KY, Lee JC, Schumm LP, Sharma Y, Anderson CA, et al. (2012). Host-microbe interactions have shaped the genetic architecture of inflammatory bowel disease. Nature 491, 119–124. 10.1038/nature11582. [PubMed: 23128233]
22. Knights D, Lassen KG, and Xavier RJ (2013). Advances in inflammatory bowel disease pathogenesis: linking host genetics and the microbiome. Gut 62, 1505–1510. 10.1136/gutjnl-2012-303954. [PubMed: 24037875]
23. Cho JH, and Abraham C (2007). Inflammatory bowel disease genetics: Nod2. Annu Rev Med 58, 401–416. 10.1146/annurev.med.58.061705.145024. [PubMed: 16987083]
24. Bonen DK, and Cho JH (2003). The genetics of inflammatory bowel disease. Gastroenterology 124, 521–536. 10.1053/gast.2003.50045. [PubMed: 12557156]
25. Kim YG, Kamada N, Shaw MH, Warner N, Chen GY, Franchi L, and Nunez G (2011). The Nod2 sensor promotes intestinal pathogen eradication via the chemokine CCL2-dependent recruitment of inflammatory monocytes. Immunity 34, 769–780. 10.1016/j.immuni.2011.04.013. [PubMed: 21565531]
26. Zhang Q, Pan Y, Yan R, Zeng B, Wang H, Zhang X, Li W, Wei H, and Liu Z (2015). Commensal bacteria direct selective cargo sorting to promote symbiosis. Nat Immunol 16, 918–926. 10.1038/ni.3233. [PubMed: 26237551]
27. Petnicki-Ocwieja T, Hrncir T, Liu YJ, Biswas A, Hudcovic T, Tlaskalova-Hogenova H, and Kobayashi KS (2009). Nod2 is required for the regulation of commensal microbiota in the intestine. Proc Natl Acad Sci U S A 106, 15813–15818. 10.1073/pnas.0907722106. [PubMed: 19805227]
28. Ramanan D, Tang MS, Bowcutt R, Loke P, and Cadwell K (2014). Bacterial sensor Nod2 prevents inflammation of the small intestine by restricting the expansion of the commensal Bacteroides vulgatus. Immunity 41, 311–324. 10.1016/j.immuni.2014.06.015. [PubMed: 25088769]
29. Marchiando AM, Ramanan D, Ding Y, Gomez LE, Hubbard-Lucey VM, Maurer K, Wang C, Ziel JW, van Rooijen N, Nunez G, et al. (2013). A deficiency in the autophagy gene Atg16L1 enhances resistance to enteric bacterial infection. Cell Host Microbe 14, 216–224. 10.1016/j.chom.2013.07.013. [PubMed: 23954160]
30. Wong SY, Coffre M, Ramanan D, Hines MJ, Gomez LE, Peters LA, Schadt EE, Koralov SB, and Cadwell K (2018). B Cell Defects Observed in Nod2 Knockout Mice Are a Consequence of a Dock2 Mutation Frequently Found in Inbred Strains. J Immunol 201, 1442–1451. 10.4049/jimmunol.1800014. [PubMed: 30012848]

31. de Souza PR, Guimaraes FR, Sales-Campos H, Bonfa G, Nardini V, Chica JEL, Turato WM, Silva JS, Zamboni DS, and Cardoso CRB (2018). Absence of NOD2 receptor predisposes to intestinal inflammation by a deregulation in the immune response in hosts that are unable to control gut dysbiosis. Immunobiology 223, 577–585. 10.1016/j.imbio.2018.07.003. [PubMed: 30041769]
32. Robertson SJ, Geddes K, Maisonneuve C, Streutker CJ, and Philpott DJ (2016). Resilience of the intestinal microbiota following pathogenic bacterial infection is independent of innate immunity mediated by NOD1 or NOD2. Microbes Infect 18, 460–471. 10.1016/j.micinf.2016.03.014. [PubMed: 27083475]
33. Geddes K, Rubino S, Streutker C, Cho JH, Magalhaes JG, Le Bourhis L, Selvanantham T, Girardin SE, and Philpott DJ (2010). Nod1 and Nod2 regulation of inflammation in the Salmonella colitis model. Infect Immun 78, 5107–5115. 10.1128/IAI.00759-10. [PubMed: 20921147]
34. Couturier-Maillard A, Secher T, Rehman A, Normand S, De Arcangelis A, Haesler R, Huot L, Grandjean T, Bressenot A, Delanoye-Crespin A, et al. (2013). NOD2-mediated dysbiosis predisposes mice to transmissible colitis and colorectal cancer. J Clin Invest 123, 700–711. 10.1172/JCI62236. [PubMed: 23281400]
35. Wehkamp J, Harder J, Weichenthal M, Schwab M, Schaffeler E, Schlee M, Herrlinger KR, Stallmach A, Noack F, Fritz P, et al. (2004). NOD2 (CARD15) mutations in Crohn's disease are associated with diminished mucosal alpha-defensin expression. Gut 53, 1658–1664. 10.1136/gut.2003.032805. [PubMed: 15479689]
36. Bevins CL, Stange EF, and Wehkamp J (2009). Decreased Paneth cell defensin expression in ileal Crohn's disease is independent of inflammation, but linked to the NOD2 1007fs genotype. Gut 58, 882–883; discussion 883–884. [PubMed: 19433600]
37. VanDussen KL, Liu TC, Li D, Towfic F, Modiano N, Winter R, Haritunians T, Taylor KD, Dhall D, Targan SR, et al. (2014). Genetic variants synthesize to produce paneth cell phenotypes that define subtypes of Crohn's disease. Gastroenterology 146, 200–209. 10.1053/j.gastro.2013.09.048. [PubMed: 24076061]
38. van Beelen Granlund A, Ostvik AE, Brenna O, Torp SH, Gustafsson BI, and Sandvik AK (2013). REG gene expression in inflamed and healthy colon mucosa explored by in situ hybridisation. Cell Tissue Res 352, 639–646. 10.1007/s00441-013-1592-z. [PubMed: 23519454]
39. Ogawa H, Fukushima K, Naito H, Funayama Y, Unno M, Takahashi K, Kitayama T, Matsuno S, Ohtani H, Takasawa S, et al. (2003). Increased expression of HIP/PAP and regenerating gene III in human inflammatory bowel disease and a murine bacterial reconstitution model. Inflamm Bowel Dis 9, 162–170. 10.1097/00054725-200305000-00003. [PubMed: 12792221]
40. Gao J, Zhao X, Hu S, Huang Z, Hu M, Jin S, Lu B, Sun K, Wang Z, Fu J, et al. (2022). Gut microbial DL-endopeptidase alleviates Crohn's disease via the NOD2 pathway. Cell Host Microbe 30, 1435–1449 e1439. 10.1016/j.chom.2022.08.002. [PubMed: 36049483]
41. Kim B, Wang YC, Hespen CW, Espinosa J, Salje J, Rangan KJ, Oren DA, Kang JY, Pedicord VA, and Hang HC (2019). Enterococcus faecium secreted antigen A generates muropeptides to enhance host immunity and limit bacterial pathogenesis. Elife 8. 10.7554/eLife.45343.
42. Kim YG, Shaw MH, Warner N, Park JH, Chen F, Ogura Y, and Nunez G (2011). Cutting edge: Crohn's disease-associated Nod2 mutation limits production of proinflammatory cytokines to protect the host from Enterococcus faecalis-induced lethality. J Immunol 187, 2849–2852. 10.4049/jimmunol.1001854. [PubMed: 21849681]
43. Garcia-Solache M, and Rice LB (2019). The Enterococcus: a Model of Adaptability to Its Environment. Clin Microbiol Rev 32. 10.1128/CMR.00058-18.
44. Balish E, and Warner T (2002). Enterococcus faecalis induces inflammatory bowel disease in interleukin-10 knockout mice. Am J Pathol 160, 2253–2257. 10.1016/S0002-9440(10)61172-8. [PubMed: 12057927]
45. Seishima J, Iida N, Kitamura K, Yutani M, Wang Z, Seki A, Yamashita T, Sakai Y, Honda M, Yamashita T, et al. (2019). Gut-derived Enterococcus faecium from ulcerative colitis patients promotes colitis in a genetically susceptible mouse host. Genome Biol 20, 252. 10.1186/s13059-019-1879-9. [PubMed: 31767028]
46. Ben Braiek O, and Smaoui S (2019). Enterococci: Between Emerging Pathogens and Potential Probiotics. Biomed Res Int 2019, 5938210. 10.1155/2019/5938210. [PubMed: 31240218]

47. Franz CM, Huch M, Abriouel H, Holzapfel W, and Galvez A (2011). Enterococci as probiotics and their implications in food safety. Int J Food Microbiol 151, 125–140. 10.1016/j.ijfoodmicro.2011.08.014. [PubMed: 21962867]
48. Rangan KJ, Pedicord VA, Wang YC, Kim B, Lu Y, Shaham S, Mucida D, and Hang HC (2016). A secreted bacterial peptidoglycan hydrolase enhances tolerance to enteric pathogens. Science 353, 1434–1437. 10.1126/science.aaf3552. [PubMed: 27708039]
49. Pedicord VA, Lockhart AAK, Rangan KJ, Craig JW, Loschko J, Rogoz A, Hang HC, and Mucida D (2016). Exploiting a host-commensal interaction to promote intestinal barrier function and enteric pathogen tolerance. Sci Immunol 1. 10.1126/sciimmunol.aai7732.
50. Griffin ME, Espinosa J, Becker JL, Luo JD, Carroll TS, Jha JK, Fanger GR, and Hang HC (2021). Enterococcus peptidoglycan remodeling promotes checkpoint inhibitor cancer immunotherapy. Science 373, 1040–1046. 10.1126/science.abc9113. [PubMed: 34446607]
51. Wang YC, Westcott NP, Griffin ME, and Hang HC (2019). Peptidoglycan Metabolite Photoaffinity Reporters Reveal Direct Binding to Intracellular Pattern Recognition Receptors and Arf GTPases. ACS Chem Biol 14, 405–414. 10.1021/acschembio.8b01038. [PubMed: 30735346]
52. Michot JM, Bigenwald C, Champiat S, Collins M, Carbonnel F, Postel-Vinay S, Berdelou A, Varga A, Bahleda R, Hollebecque A, et al. (2016). Immune-related adverse events with immune checkpoint blockade: a comprehensive review. Eur J Cancer 54, 139–148. 10.1016/j.ejca.2015.11.016. [PubMed: 26765102]
53. Parikh A, Stephan AF, and Tzanakakis ES (2012). Regenerating proteins and their expression, regulation and signaling. Biomol Concepts 3, 57–70. 10.1515/bmc.2011.055. [PubMed: 22582090]
54. Wang W, Wang Y, Lu Y, Zhu J, Tian X, Wu B, Du J, Cai W, and Xiao Y (2022). Reg4 protects against Salmonella infection-associated intestinal inflammation via adopting a calcium-dependent lectin-like domain. Int Immunopharmacol 113, 109310. 10.1016/j.intimp.2022.109310. [PubMed: 36274484]
55. Qi H, Wei J, Gao Y, Yang Y, Li Y, Zhu H, Su L, Su X, Zhang Y, and Yang R (2020). Reg4 and complement factor D prevent the overgrowth of E. coli in the mouse gut. Commun Biol 3, 483. 10.1038/s42003-020-01219-2. [PubMed: 32879431]
56. Bradley CR, and Fraise AP (1996). Heat and chemical resistance of enterococci. J Hosp Infect 34, 191–196. 10.1016/s0195-6701(96)90065-1. [PubMed: 8923273]
57. McHugh CP, Zhang P, Michalek S, and Eleazer PD (2004). pH required to kill Enterococcus faecalis in vitro. J Endod 30, 218–219. 10.1097/00004770-200404000-00008. [PubMed: 15085049]
58. Maria R, Dutta SD, Thete SG, and AlAttas MH (2021). Evaluation of Antibacterial Properties of Organic Gutta-percha Solvents and Synthetic Solvents Against Enterococcus faecalis. J Int Soc Prev Community Dent 11, 179–183. 10.4103/jispcd.JISPCD_422_20. [PubMed: 34036080]
59. Luddin N, and Ahmed HM (2013). The antibacterial activity of sodium hypochlorite and chlorhexidine against Enterococcus faecalis: A review on agar diffusion and direct contact methods. J Conserv Dent 16, 9–16. 10.4103/0972-0707.105291. [PubMed: 23349569]
60. Piewngam P, Zheng Y, Nguyen TH, Dickey SW, Joo HS, Villaruz AE, Glose KA, Fisher EL, Hunt RL, Li B, et al. (2018). Pathogen elimination by probiotic Bacillus via signalling interference. Nature 562, 532–537. 10.1038/s41586-018-0616-y. [PubMed: 30305736]
61. Hall AB, Yassour M, Sauk J, Garner A, Jiang X, Arthur T, Lagoudas GK, Vatanen T, Fornelos N, Wilson R, et al. (2017). A novel Ruminococcus gnavus clade enriched in inflammatory bowel disease patients. Genome Med 9, 103. 10.1186/s13073-017-0490-5. [PubMed: 29183332]
62. Lewis JD, Chen EZ, Baldassano RN, Otley AR, Griffiths AM, Lee D, Bittinger K, Bailey A, Friedman ES, Hoffmann C, et al. (2015). Inflammation, Antibiotics, and Diet as Environmental Stressors of the Gut Microbiome in Pediatric Crohn's Disease. Cell Host Microbe 18, 489–500. 10.1016/j.chom.2015.09.008. [PubMed: 26468751]
63. Franzosa EA, Sirota-Madi A, Avila-Pacheco J, Fornelos N, Haiser HJ, Reinker S, Vatanen T, Hall AB, Mallick H, McIver LJ, et al. (2019). Gut microbiome structure and metabolic activity in inflammatory bowel disease. Nat Microbiol 4, 293–305. 10.1038/s41564-018-0306-4. [PubMed: 30531976]

64. Chassaing B, Srinivasan G, Delgado MA, Young AN, Gewirtz AT, and Vijay-Kumar M (2012). Fecal lipocalin 2, a sensitive and broadly dynamic non-invasive biomarker for intestinal inflammation. PLoS One 7, e44328. 10.1371/journal.pone.0044328. [PubMed: 22957064]

65. Forster SC, Clare S, Beresford-Jones BS, Harcourt K, Notley G, Stares MD, Kumar N, Soderholm AT, Adoum A, Wong H, et al. (2022). Identification of gut microbial species linked with disease variability in a widely used mouse model of colitis. Nat Microbiol 7, 590–599. 10.1038/s41564-022-01094-z. [PubMed: 35365791]

66. Moon C, Baldridge MT, Wallace MA, Burnham D,CA, Virgin HW, and Stappenbeck TS (2015). Vertically transmitted faecal IgA levels determine extra-chromosomal phenotypic variation. Nature 521, 90–93. 10.1038/nature14139. [PubMed: 25686606]

67. Kommineni S, Bretl DJ, Lam V, Chakraborty R, Hayward M, Simpson P, Cao Y, Bousounis P, Kristich CJ, and Salzman NH (2015). Bacteriocin production augments niche competition by enterococci in the mammalian gastrointestinal tract. Nature 526, 719–722. 10.1038/nature15524. [PubMed: 26479034]

68. Chen Z, Downing S, and Tzanakakis ES (2019). Four Decades After the Discovery of Regenerating Islet-Derived (Reg) Proteins: Current Understanding and Challenges. Front Cell Dev Biol 7, 235. 10.3389/fcell.2019.00235. [PubMed: 31696115]

69. Edwards JA, Tan N, Toussaint N, Ou P, Mueller C, Stanek A, Zinsou V, Roudnitsky S, Sagal M, Dresner L, et al. (2020). Role of regenerating islet-derived proteins in inflammatory bowel disease. World J Gastroenterol 26, 2702–2714. 10.3748/wjg.v26.i21.2702. [PubMed: 32550748]

70. Teng F, Kawalec M, Weinstock GM, Hryniewicz W, and Murray BE (2003). An Enterococcus faecium secreted antigen, SagA, exhibits broad-spectrum binding to extracellular matrix proteins and appears essential for E. faecium growth. Infect Immun 71, 5033–5041. 10.1128/IAI.71.9.5033-5041.2003. [PubMed: 12933846]

71. Rakoff-Nahoum S, Paglino J, Eslami-Varzaneh F, Edberg S, and Medzhitov R (2004). Recognition of commensal microflora by toll-like receptors is required for intestinal homeostasis. Cell 118, 229–241. 10.1016/j.cell.2004.07.002. [PubMed: 15260992]

72. Kernbauer E, Ding Y, and Cadwell K (2014). An enteric virus can replace the beneficial function of commensal bacteria. Nature 516, 94–98. 10.1038/nature13960. [PubMed: 25409145]

73. Ferrand A, Al Nabhani Z, Tapias NS, Mas E, Hugot JP, and Barreau F (2019). NOD2 Expression in Intestinal Epithelial Cells Protects Toward the Development of Inflammation and Associated Carcinogenesis. Cell Mol Gastroenterol Hepatol 7, 357–369. 10.1016/j.jcmgh.2018.10.009. [PubMed: 30704984]

74. Mukherjee T, Hovingh ES, Foerster EG, Abdel-Nour M, Philpott DJ, and Girardin SE (2019). NOD1 and NOD2 in inflammation, immunity and disease. Arch Biochem Biophys 670, 69–81. 10.1016/j.abb.2018.12.022. [PubMed: 30578751]

75. Trindade BC, and Chen GY (2020). NOD1 and NOD2 in inflammatory and infectious diseases. Immunol Rev 297, 139–161. 10.1111/imr.12902. [PubMed: 32677123]

76. Neil JA, Matsuzawa-Ishimoto Y, Kernbauer-Holzl E, Schuster SL, Sota S, Venzon M, Dallari S, Galvao Neto A, Hine A, Hudesman D, et al. (2019). IFN-I and IL-22 mediate protective effects of intestinal viral infection. Nat Microbiol 4, 1737–1749. 10.1038/s41564-019-0470-1. [PubMed: 31182797]

77. Sugimoto K, Ogawa A, Mizoguchi E, Shimomura Y, Andoh A, Bhan AK, Blumberg RS, Xavier RJ, and Mizoguchi A (2008). IL-22 ameliorates intestinal inflammation in a mouse model of ulcerative colitis. J Clin Invest 118, 534–544. 10.1172/JCI33194. [PubMed: 18172556]

78. Chu H, Khosravi A, Kusumawardhani IP, Kwon AH, Vasconcelos AC, Cunha LD, Mayer AE, Shen Y, Wu WL, Kambal A, et al. (2016). Gene-microbiota interactions contribute to the pathogenesis of inflammatory bowel disease. Science 352, 1116–1120. 10.1126/science.aad9948. [PubMed: 27230380]

79. Wu WH, Kim M, Chang LC, Assie A, Saldana-Morales FB, Zegarra-Ruiz DF, Norwood K, Samuel BS, and Diehl GE (2022). Interleukin-1beta secretion induced by mucosa-associated gut commensal bacteria promotes intestinal barrier repair. Gut Microbes 14, 2014772. 10.1080/19490976.2021.2014772. [PubMed: 34989321]

80. Seo SU, Kuffa P, Kitamoto S, Nagao-Kitamoto H, Rousseau J, Kim YG, Nunez G, and Kamada N (2015). Intestinal macrophages arising from CCR2(+) monocytes control pathogen infection by activating innate lymphoid cells. Nat Commun 6, 8010. 10.1038/ncomms9010. [PubMed: 26269452]

81. Zhou L, Chu C, Teng F, Bessman NJ, Goc J, Santosa EK, Putzel GG, Kabata H, Kelsen JR, Baldassano RN, et al. (2019). Innate lymphoid cells support regulatory T cells in the intestine through interleukin-2. Nature 568, 405–409. 10.1038/s41586-019-1082-x. [PubMed: 30944470]

82. Ebbo M, Crinier A, Vely F, and Vivier E (2017). Innate lymphoid cells: major players in inflammatory diseases. Nat Rev Immunol 17, 665–678. 10.1038/nri.2017.86. [PubMed: 28804130]

83. Mizoguchi A, Yano A, Himuro H, Ezaki Y, Sadanaga T, and Mizoguchi E (2018). Clinical importance of IL-22 cascade in IBD. J Gastroenterol 53, 465–474. 10.1007/s00535-017-1401-7. [PubMed: 29075900]

84. Swanson KV, Deng M, and Ting JP (2019). The NLRP3 inflammasome: molecular activation and regulation to therapeutics. Nat Rev Immunol 19, 477–489. 10.1038/s41577-019-0165-0. [PubMed: 31036962]

85. Huang Y, Xu W, and Zhou R (2021). NLRP3 inflammasome activation and cell death. Cell Mol Immunol 18, 2114–2127. 10.1038/s41423-021-00740-6. [PubMed: 34321623]

86. Bauernfeind FG, Horvath G, Stutz A, Alnemri ES, MacDonald K, Speert D, Fernandes-Alnemri T, Wu J, Monks BG, Fitzgerald KA, et al. (2009). Cutting edge: NF-kappaB activating pattern recognition and cytokine receptors license NLRP3 inflammasome activation by regulating NLRP3 expression. J Immunol 183, 787–791. 10.4049/jimmunol.0901363. [PubMed: 19570822]

87. Yao X, Zhang C, Xing Y, Xue G, Zhang Q, Pan F, Wu G, Hu Y, Guo Q, Lu A, et al. (2017). Remodelling of the gut microbiota by hyperactive NLRP3 induces regulatory T cells to maintain homeostasis. Nat Commun 8, 1896. 10.1038/s41467-017-01917-2. [PubMed: 29196621]

88. Zhu Q, and Kanneganti TD (2017). Cutting Edge: Distinct Regulatory Mechanisms Control Proinflammatory Cytokines IL-18 and IL-1beta. J Immunol 198, 4210–4215. 10.4049/jimmunol.1700352. [PubMed: 28468974]

89. Inohara N, Ogura Y, Fontalba A, Gutierrez O, Pons F, Crespo J, Fukase K, Inamura S, Kusumoto S, Hashimoto M, et al. (2003). Host recognition of bacterial muramyl dipeptide mediated through NOD2. Implications for Crohn's disease. J Biol Chem 278, 5509–5512. 10.1074/jbc.C200673200. [PubMed: 12514169]

90. Hugot JP, Chamaillard M, Zouali H, Lesage S, Cezard JP, Belaiche J, Almer S, Tysk C, O'Morain CA, Gassull M, et al. (2001). Association of NOD2 leucine-rich repeat variants with susceptibility to Crohn's disease. Nature 411, 599–603. 10.1038/35079107. [PubMed: 11385576]

91. Murano T, Okamoto R, Ito G, Nakata T, Hibiya S, Shimizu H, Fujii S, Kano Y, Mizutani T, Yui S, et al. (2014). Hes1 promotes the IL-22-mediated antimicrobial response by enhancing STAT3-dependent transcription in human intestinal epithelial cells. Biochem Biophys Res Commun 443, 840–846. 10.1016/j.bbrc.2013.12.061. [PubMed: 24342613]

92. Loonen LM, Stolte EH, Jaklofsky MT, Meijerink M, Dekker J, van Baarlen P, and Wells JM (2014). REG3gamma-deficient mice have altered mucus distribution and increased mucosal inflammatory responses to the microbiota and enteric pathogens in the ileum. Mucosal Immunol 7, 939–947. 10.1038/mi.2013.109. [PubMed: 24345802]

93. Winter SE, Winter MG, Xavier MN, Thiennimitr P, Poon V, Keestra AM, Laughlin RC, Gomez G, Wu J, Lawhon SD, et al. (2013). Host-derived nitrate boosts growth of E. coli in the inflamed gut. Science 339, 708–711. 10.1126/science.1232467. [PubMed: 23393266]

94. Lee JY, Tsolis RM, and Baumler AJ (2022). The microbiome and gut homeostasis. Science 377, eabp9960. 10.1126/science.abp9960. [PubMed: 35771903]

95. Shouval DS, Biswas A, Kang YH, Griffith AE, Konnikova L, Mascanfroni ID, Redhu NS, Frei SM, Field M, Doty AL, et al. (2016). Interleukin 1beta Mediates Intestinal Inflammation in Mice and Patients With Interleukin 10 Receptor Deficiency. Gastroenterology 151, 1100–1104. 10.1053/j.gastro.2016.08.055. [PubMed: 27693323]

96. Kim D, Kim YG, Seo SU, Kim DJ, Kamada N, Prescott D, Chamaillard M, Philpott DJ, Rosenstiel P, Inohara N, and Nunez G (2016). Nod2-mediated recognition of the microbiota is critical for

mucosal adjuvant activity of cholera toxin. Nat Med 22, 524–530. 10.1038/nm.4075. [PubMed: 27064448]

97. Martin PK, Marchiando A, Xu R, Rudensky E, Yeung F, Schuster SL, Kernbauer E, and Cadwell K (2018). Autophagy proteins suppress protective type I interferon signalling in response to the murine gut microbiota. Nat Microbiol 3, 1131–1141. 10.1038/s41564-018-0229-0. [PubMed: 30202015]
98. Matsuzawa-Ishimoto Y, Yao X, Koide A, Ueberheide BM, Axelrad JE, Reis BS, Parsa R, Neil JA, Devlin JC, Rudensky E, et al. (2022). The gammadelta IEL effector API5 masks genetic susceptibility to Paneth cell death. Nature 610, 547–554. 10.1038/s41586-022-05259-y. [PubMed: 36198790]
99. Schindelin J, Arganda-Carreras I, Frise E, Kaynig V, Longair M, Pietzsch T, Preibisch S, Rueden C, Saalfeld S, Schmid B, et al. (2012). Fiji: an open-source platform for biological-image analysis. Nat Methods 9, 676–682. 10.1038/nmeth.2019. [PubMed: 22743772]
100. Bokulich NA, Kaehler BD, Rideout JR, Dillon M, Bolyen E, Knight R, Huttley GA, and Gregory Caporaso J (2018). Optimizing taxonomic classification of marker-gene amplicon sequences with QIIME 2's q2-feature-classifier plugin. Microbiome 6, 90. 10.1186/s40168-018-0470-z. [PubMed: 29773078]
101. Lozupone C, Lladser ME, Knights D, Stombaugh J, and Knight R (2011). UniFrac: an effective distance metric for microbial community comparison. ISME J 5, 169–172. 10.1038/ismej.2010.133. [PubMed: 20827291]
102. Vazquez-Baeza Y, Pirrung M, Gonzalez A, and Knight R (2013). EMPeror: a tool for visualizing high-throughput microbial community data. Gigascience 2, 16. 10.1186/2047-217X-2-16. [PubMed: 24280061]
103. Mandal S, Van Treuren W, White RA, Eggesbo M, Knight R, and Peddada SD (2015). Analysis of composition of microbiomes: a novel method for studying microbial composition. Microb Ecol Health Dis 26, 27663. 10.3402/mehd.v26.27663. [PubMed: 26028277]
104. Cheng S, McCleskey FK, Gress MJ, Petroziello JM, Liu R, Namdari H, Beninga K, Salmen A, and DelVecchio VG (1997). A PCR assay for identification of Enterococcus faecium. J Clin Microbiol 35, 1248–1250. 10.1128/jcm.35.5.1248-1250.1997. [PubMed: 9114416]
105. Chen S, Zhou Y, Chen Y, and Gu J (2018). fastp: an ultra-fast all-in-one FASTQ preprocessor. Bioinformatics 34, i884–i890. 10.1093/bioinformatics/bty560. [PubMed: 30423086]
106. Low AJ, Koziol AG, Manninger PA, Blais B, and Carrillo CD (2019). ConFindr: rapid detection of intraspecies and cross-species contamination in bacterial whole-genome sequence data. PeerJ 7, e6995. 10.7717/peerj.6995. [PubMed: 31183253]
107. Chaumeil PA, Mussig AJ, Hugenholtz P, and Parks DH (2019). GTDB-Tk: a toolkit to classify genomes with the Genome Taxonomy Database. Bioinformatics 36, 1925–1927. 10.1093/bioinformatics/btz848. [PubMed: 31730192]
108. Wick RR, Judd LM, Gorrie CL, and Holt KE (2017). Unicycler: Resolving bacterial genome assemblies from short and long sequencing reads. PLoS Comput Biol 13, e1005595. 10.1371/journal.pcbi.1005595. [PubMed: 28594827]
109. Altschul SF, Gish W, Miller W, Myers EW, and Lipman DJ (1990). Basic local alignment search tool. J Mol Biol 215, 403–410. 10.1016/S0022-2836(05)80360-2. [PubMed: 2231712]
110. Stamatakis A (2014). RAxML version 8: a tool for phylogenetic analysis and post-analysis of large phylogenies. Bioinformatics 30, 1312–1313. 10.1093/bioinformatics/btu033. [PubMed: 24451623]
111. Csardi G, and Nepusz T The igraph software package for complex network research.
112. Vandesompele J, De Preter K, Pattyn F, Poppe B, Van Roy N, De Paepe A, and Speleman F (2002). Accurate normalization of real-time quantitative RT-PCR data by geometric averaging of multiple internal control genes. Genome Biol 3, RESEARCH0034. 10.1186/gb-2002-3-7-research0034. [PubMed: 12184808]
113. Dallari S, Heaney T, Rosas-Villegas A, Neil JA, Wong SY, Brown JJ, Urbanek K, Herrmann C, Depledge DP, Dermody TS, and Cadwell K (2021). Enteric viruses evoke broad host immune responses resembling those elicited by the bacterial microbiome. Cell Host Microbe 29, 1014–1029 e1018. 10.1016/j.chom.2021.03.015. [PubMed: 33894129]

114. Jang KK, Kaczmarek ME, Dallari S, Chen YH, Tada T, Axelrad J, Landau NR, Stapleford KA, and Cadwell K (2022). Variable susceptibility of intestinal organoid-derived monolayers to SARS-CoV-2 infection. PLoS Biol 20, e3001592. 10.1371/journal.pbio.3001592. [PubMed: 35358182]

Highlights

- REG3 proteins deplete *Enterococcus faecium* in gut microbiota of IBD patients
- *E. faecium* SagA inhibits intestinal inflammation in a NOD2-dependent manner
- NOD2 activated myeloid cells produce IL-1β to induce IL-22 from lymphoid cells
- The NOD2 R702W variant impairs *E. faecium*-mediated protection in mice

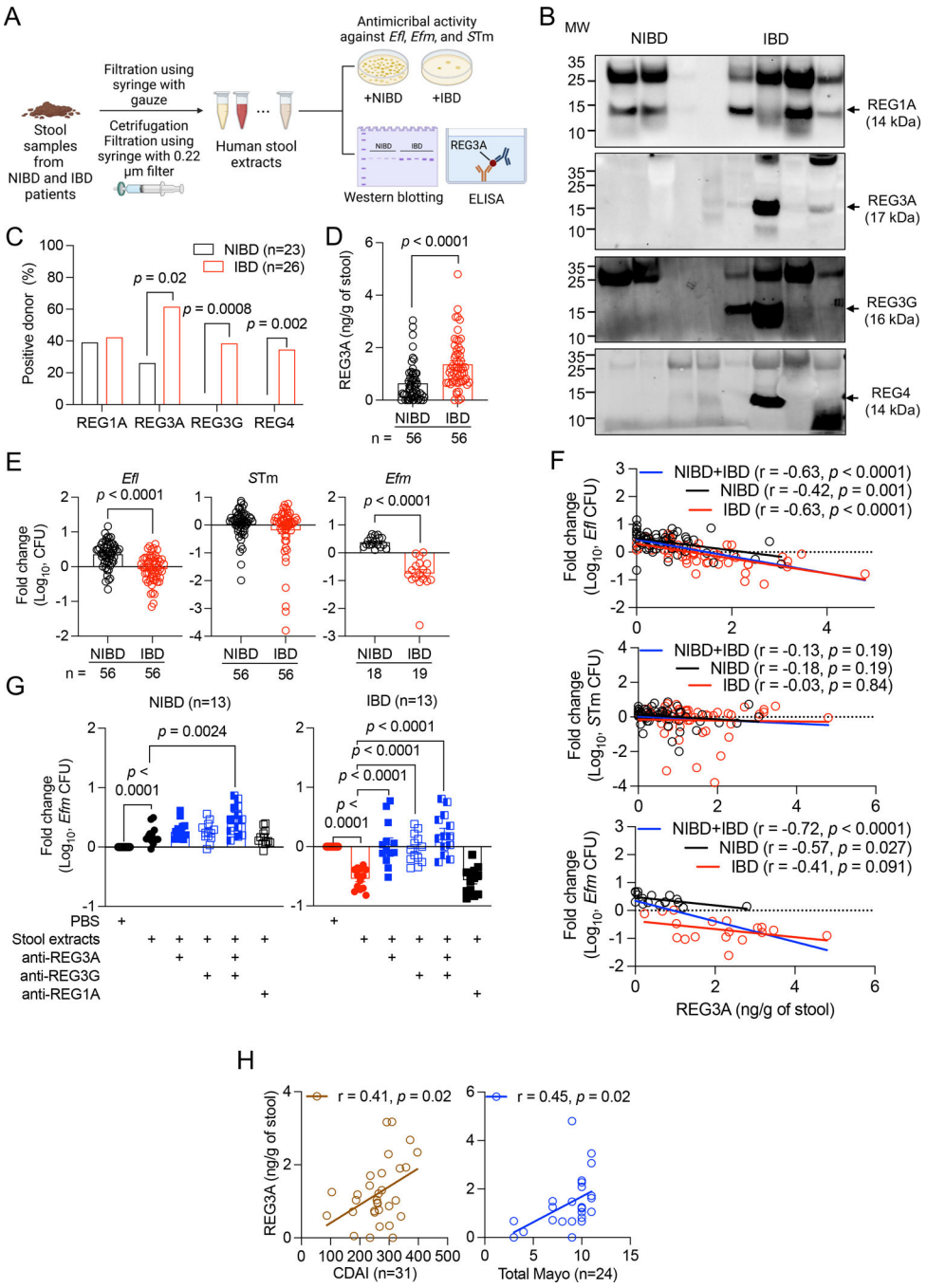

Figure 1. Increased REG3A and REG3G in IBD patient stool inhibit *Enterococcus*.

A) Schematic of stool extract preparation and analysis. **B)** Western blots of REG1A, REG3A, REG3G, and REG4 in stool extracts from representative 3 non-IBD (NIBD) and 5 IBD patients. **C)** Proportion of specimens from NIBD and IBD patients in which REG1A, REG3A, REG3G, or REG4 were detectable by western blot. **D)** Quantification of REG3A in NIBD and IBD stool extracts by ELISA. **E)** Fold changes in colony forming unit (CFU) of *Enterococcus faecalis* (*Efl*) and *Salmonella* Typhimurium (*S*Tm) cultured in NIBD and IBD stool extracts. Results obtained with *Efl* were confirmed with *E. faecium* (*Efm*). **F)**

Correlation between REG3A concentration and CFU fold changes of *Efl* (upper), *S*Tm (middle), and *Efm* (lower) cultured in NIBD and IBD stool extract. **G)** Fold change in *Efm* CFU cultured in PBS or NIBD (left) and IBD (right) stool extracts in the presence of indicated antibodies. **H)** Correlation between REG3A concentration and Crohn's disease activity index (CDAI) for CD patients or total Mayo score for ulcerative colitis (UC) patients. Data points in D-H represent individual patients. Bars represent mean ± SEM and at least three independent experiments were performed. r, Pearson correlation coefficient. Indicated *p* values by Fisher's exact test in C, unpaired *t* test, two-tailed in D, E, and G, and simple linear regression analysis in F and H. See also Figure S1 and Tables S1–S3.

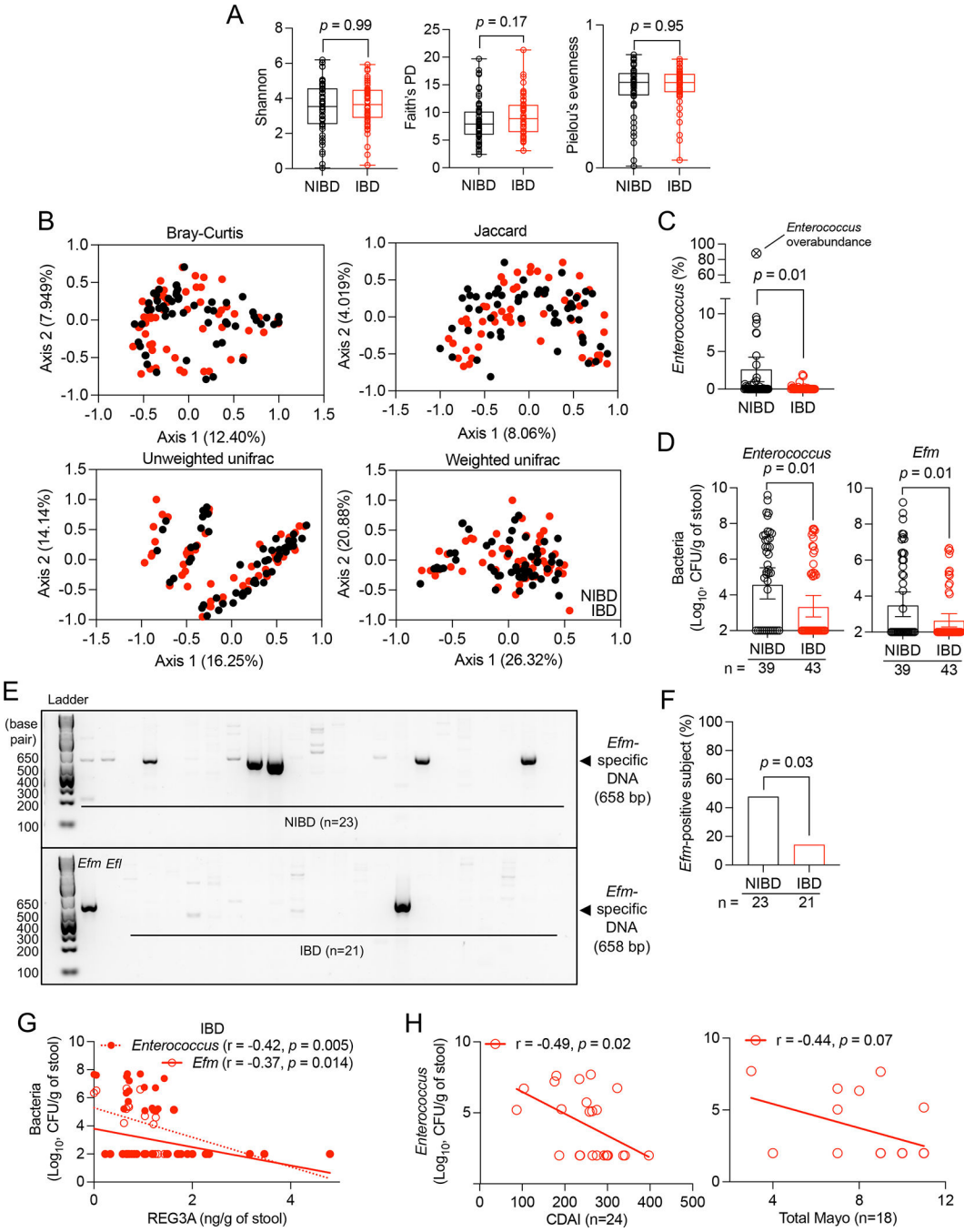

Figure 2. *Enterococcus* and *Efm* are depleted in gut microbiota from IBD patients.

A and B) 16S rRNA sequencing of stool from NIBD and IBD patients from Figure 1. Alpha diversity calculated by Shannon, Faith's phylogenetic diversity (PD), and Pielou's evenness indices (A). Principle coordinate analyses of beta diversity determined by Bray-Curtis, Jaccard, and Unweighted and Weighted unifrac methods (B). **C)** Proportion of sequencing reads representing *Enterococcus* in NIBD and IBD patient stool. One NIBD sample contained >80% *Enterococcus*, which is shown as a reference on the graph but excluded from statistical analysis and downstream assays. **D)** Total *Enterococcus* and *Efm*

CFUs in NIBD and IBD specimens. **E)** Gel image of *Efm* detected by PCR in stool DNA. Genomic DNA isolated from *Efm* and *Efl* in the first two lanes of the bottom panel serves as positive and negative controls, respectively. **F)** Proportion of NIBD and IBD patients in which *Efm* was detectable by PCR. **G)** Correlation between REG3A concentration and total *Enterococcus* and *Efm* CFUs in IBD stool. **H)** Correlation between *Enterococcus* CFUs and CDAI and total Mayo score. Data points in A-D, G, and H represent individual patients. Bars represent mean ± SEM from at least three independent experiments. r, Pearson correlation coefficient. Indicated *p* values by Kruskal-Wallis test in A, unpaired *t* test, two-tailed in C and D, Fisher's exact test in F, and simple linear regression analysis in G and H. See also Figure S1 and Tables S1–S3.

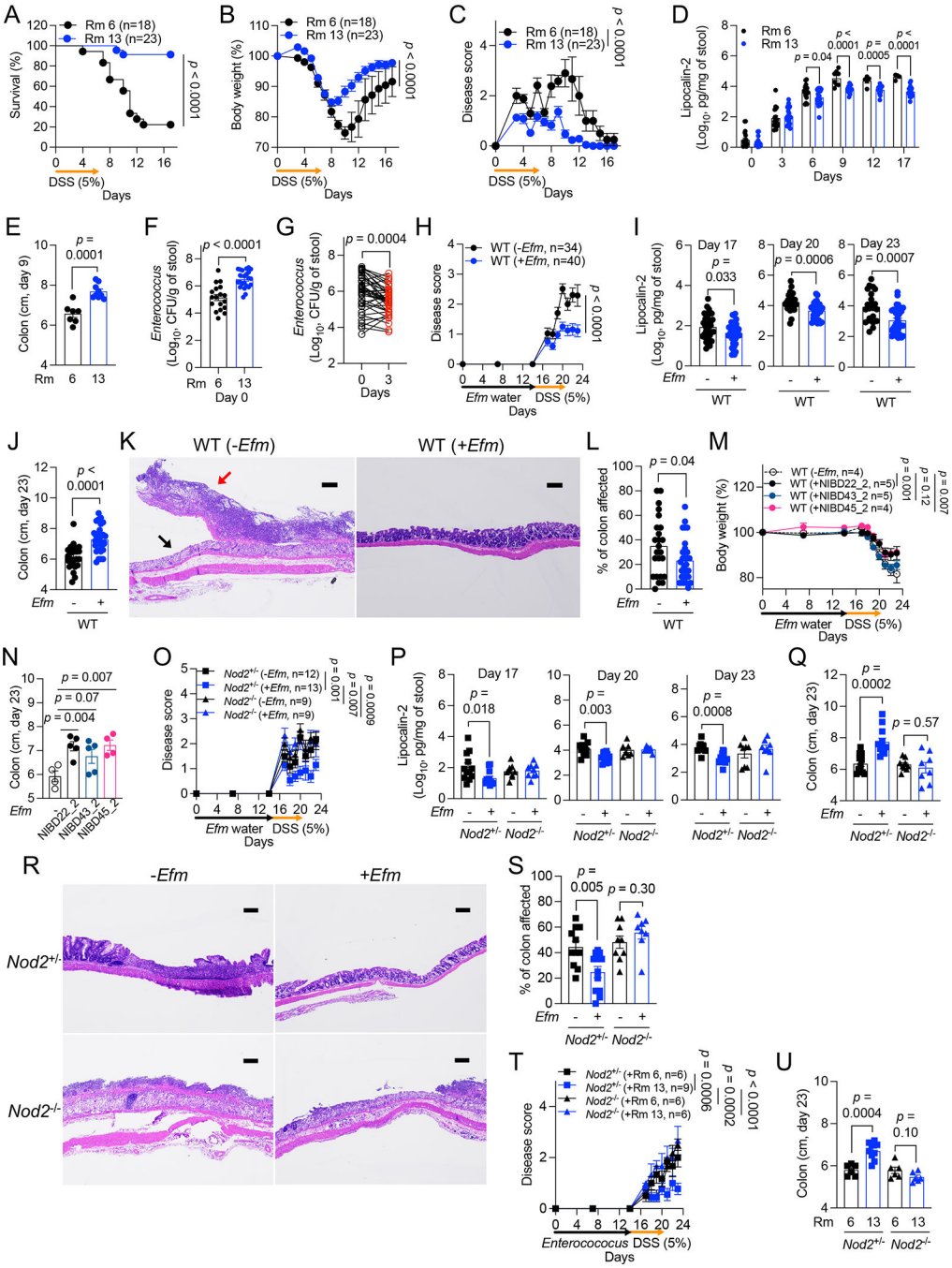

Figure 3. *Enterococcus* protects against intestinal injury through NOD2.

A-G) Dextran sulfate sodium (DSS)-induced intestinal injury of wild-type (WT) B6 mice bred in room 6 (Rm 6) or 13 (Rm 13). Mice were examined for survival (A), changes in body weight (B) disease score (C), fecal lipocalin-2 (LCN2) (D), colon length on day 9 (E), endogenous *Enterococcus* burden on day 0 (F), and changes in *Enterococcus* burden on day 3 (G). **H-L)** DSS treatment of WT mice from Rm 6 following administration of *Efm* or control. Mice were examined for changes in disease score (H), fecal LCN2 (I), and colon length on day 23 (J). Representative images of hematoxylin and eosin (H&E)-

stained sections of the colon (K) and quantification of the proportion of colon affected (L). Black arrow indicates destroyed colonic epithelium replaced with a diffuse ulcer and pus; red arrow indicates acute inflammation with primary neutrophils, lymphocytes, plasma cells, and dead cell debris. Breakdown of histological measurements by individual mice is provided in Table S4 for this and other figures. **M and N)** Body weight change (M) and colon length on day 23 (N) after DSS treatment of WT mice from Rm 6 following administration of *Efm* isolates from NIBD patients. **O-S)** DSS treatment of *Nod2*$^{+/-}$ and *Nod2*$^{-/-}$ mice from Rm 6 following administration of *Efm* or control. Mice were examined for changes in disease score (O), fecal LCN2 at indicated time points (P), and colon length on day 23 (Q). Representative images of H&E-stained sections of the colon (R) and quantification of the proportion of colon affected (S). **T and U)** Disease score (T) and colon length on day 23 (U) after DSS treatment of *Nod2*$^{+/-}$ and *Nod2*$^{-/-}$ mice following administration of *Enterococcus* isolated from Rm 6 or Rm 13. Bars, 200 μm. Data points in D-G, I, J, L, N, P, Q, S, and U represent individual mice. Data points in B, C, H, M, O, and T represent mean ± SEM. Bars represent mean ± SEM from at least two independent experiments. Indicated *p* values by log-rank Mantel-Cox test in A, two-way ANOVA test in B, C, H, M, O, and T, unpaired *t* test, two-tailed in D-F, I, J, L, N, P, Q, S, and U, and paired *t* test, two-tailed in G. See also Figures S2 and S3 and Table S4.

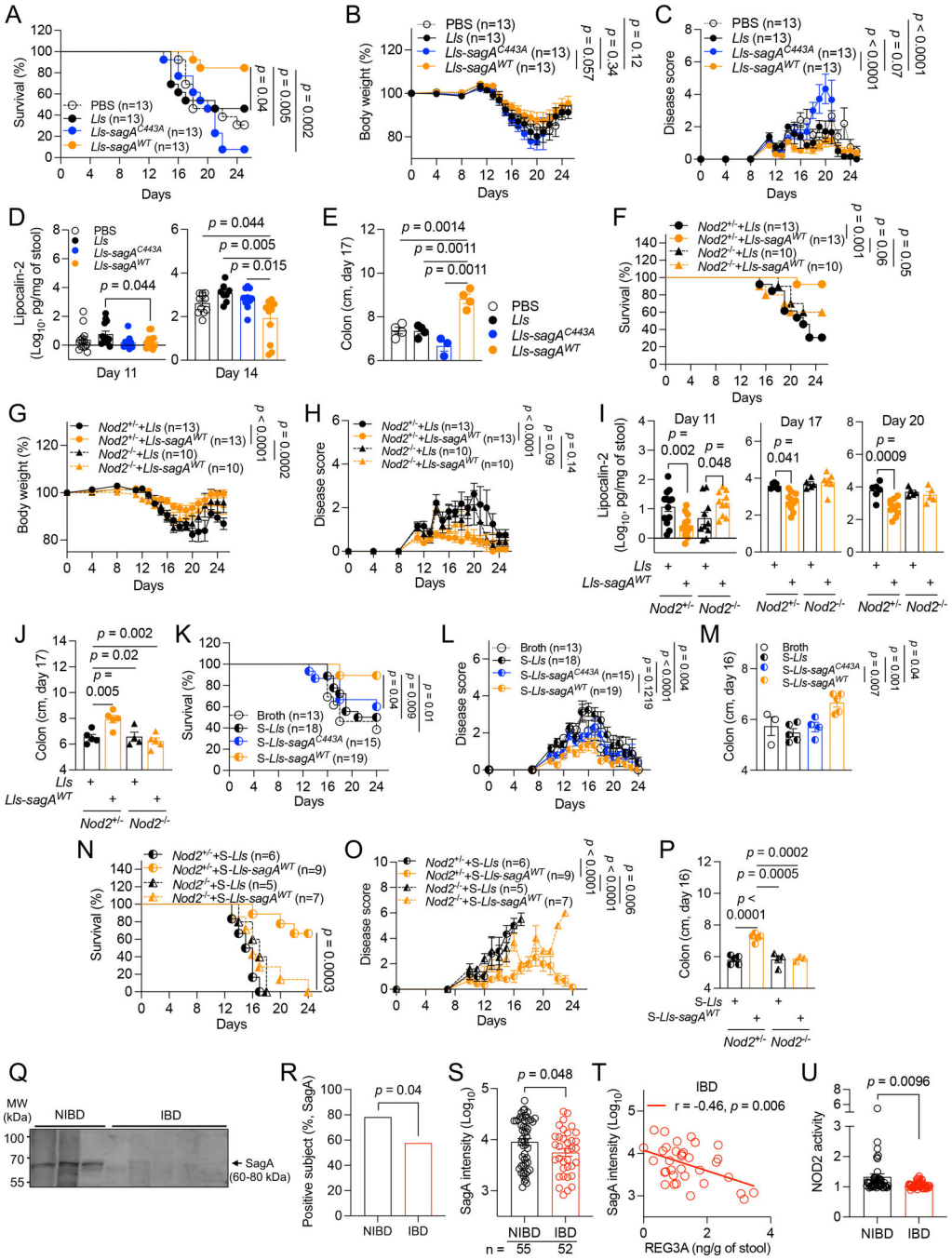

Figure 4. SagA mediates NOD2-dependent protection against intestinal injury.

A-E) Antibiotics (abx)-treated WT mice orally inoculated with PBS, *Lactococcus lactis* (*Lls*), *Lls-sagA*^{WT}, or *Lls-sagA*^{C443A} and given DSS were examined for survival (A), changes in body weight (B), disease score (C), fecal LCN2 (D), and colon length on day 17 (E). **F-J)** Abx-treated *Nod2*$^{+/-}$ and *Nod2*$^{-/-}$ mice inoculated with *Lls* or *Lls-sagA*^{WT} and given DSS were examined for survival (F), changes in body weight (G) and disease score (H), fecal LCN2 (I), and colon length on day 17 (J). **K-M)** DSS-treated WT mice receiving broth or culture supernatants of *Lls* (S-*Lls*), *Lls-sagA*^{WT} (S-*Lls-sagA*^{WT}), or *Lls-sagA*^{C443A}

(S-*Lls-sagA*^{C443A}) in drinking water were examined for survival (K), changes in disease score (L), and colon length on day 16 (M). **N-P)** DSS-treated *Nod2*$^{+/-}$ and *Nod2*$^{-/-}$ mice receiving S-*Lls* or S-*Lls-sagA*^{WT} were examined for survival (N), changes in disease score (O), and colon length on day 16 (P). **Q)** Western blots of SagA in stool extracts from representative 3 NIBD and 5 IBD patients. **R and S)** Proportion of NIBD and IBD patients in which SagA was detectable by western blot (R) and band intensity (S). **T)** Correlation between SagA and REG3A. **U)** NOD2 activity detected by HEK-Blue NOD2 reporter cells incubated with NIBD and IBD stool extracts. Values represent fold change over background control cells. Data points in D, E, I, J, M, and P represent individual mice. Data points in S-U represent individual patients. Data points in B, C, G, H, L, and O represent mean ± SEM. Bars represent mean ± SEM from at least two independent experiments. r, Pearson correlation coefficient. Indicated *p* values by log-rank Mantel-Cox test in A, F, K, and N, two-way ANOVA test in B, C, G, H, L, and O, unpaired *t* test, two-tailed in D, E, I, J, M, P, S, and U, Fisher's exact test in R, and simple linear regression analysis in T. See also Figure S4 and Tables S1 and S2.

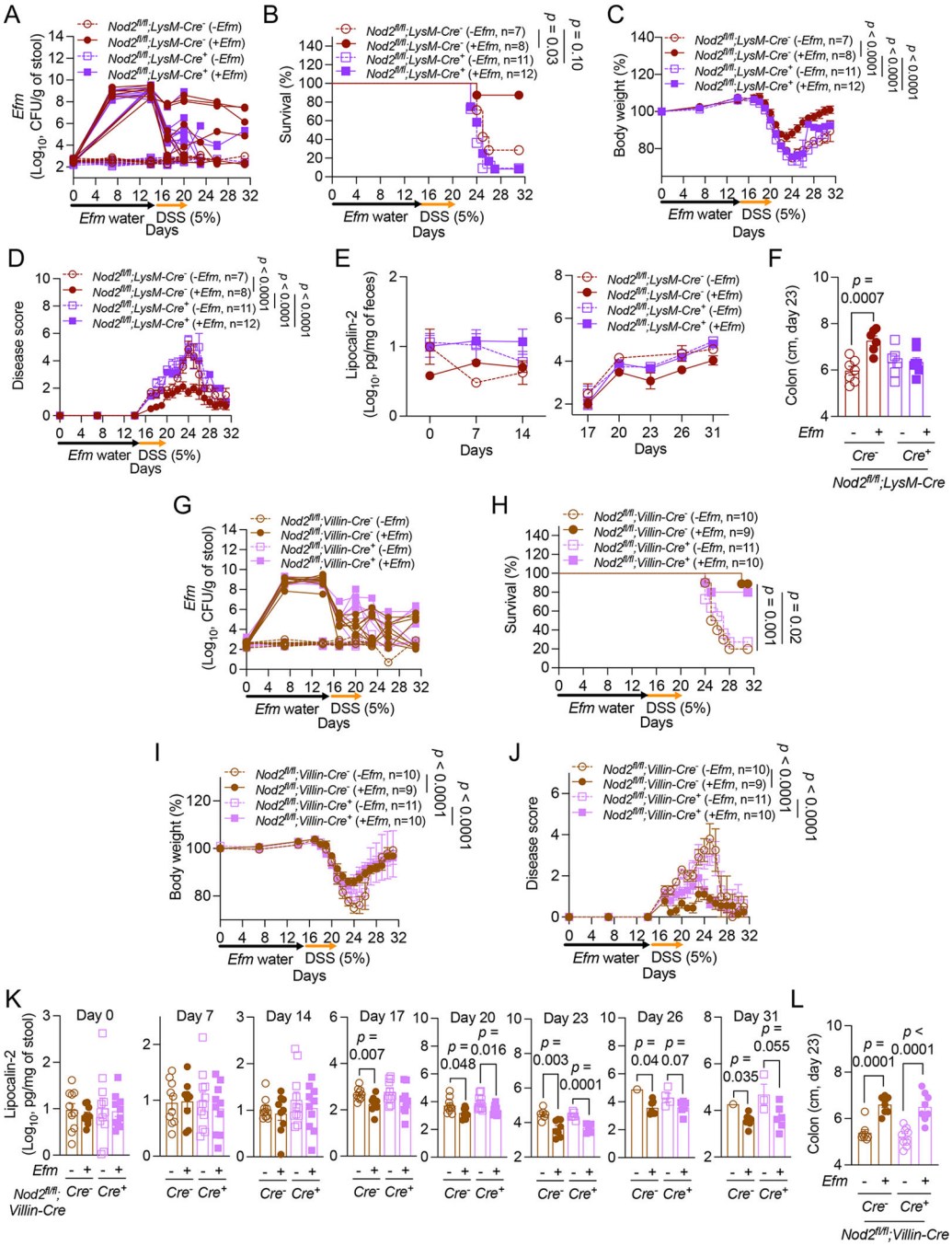

Figure 5. NOD2 in myeloid cells is required for *Efm*-mediated protection.

A-L) DSS-treated *Nod2*$^{fl/fl}$*;LysM-Cre*$^{-}$ and *Cre*$^{+}$ mice (A-F) or *Nod2*$^{fl/fl}$*;Villin-Cre*$^{-}$ and *Cre*$^{+}$ mice (G-L) following administration of *Efm* or control were examined for *Efm* burden in stool (A and G), survival (B and H), changes in body weight (C and I), disease score (D and J), fecal LCN2 (E and K), and colon length on day 23 (F and L). Lines in A and G and data points in F, K, and L represent Individual mice. Data points in C-E, I, and J represent mean ± SEM. Bars represent mean ± SEM from at least three independent experiments.

Indicated *p* values by log-rank Mantel-Cox test in B and H, two-way ANOVA test in C, D, I, and J, and unpaired *t* test, two-tailed in F, K, and L.

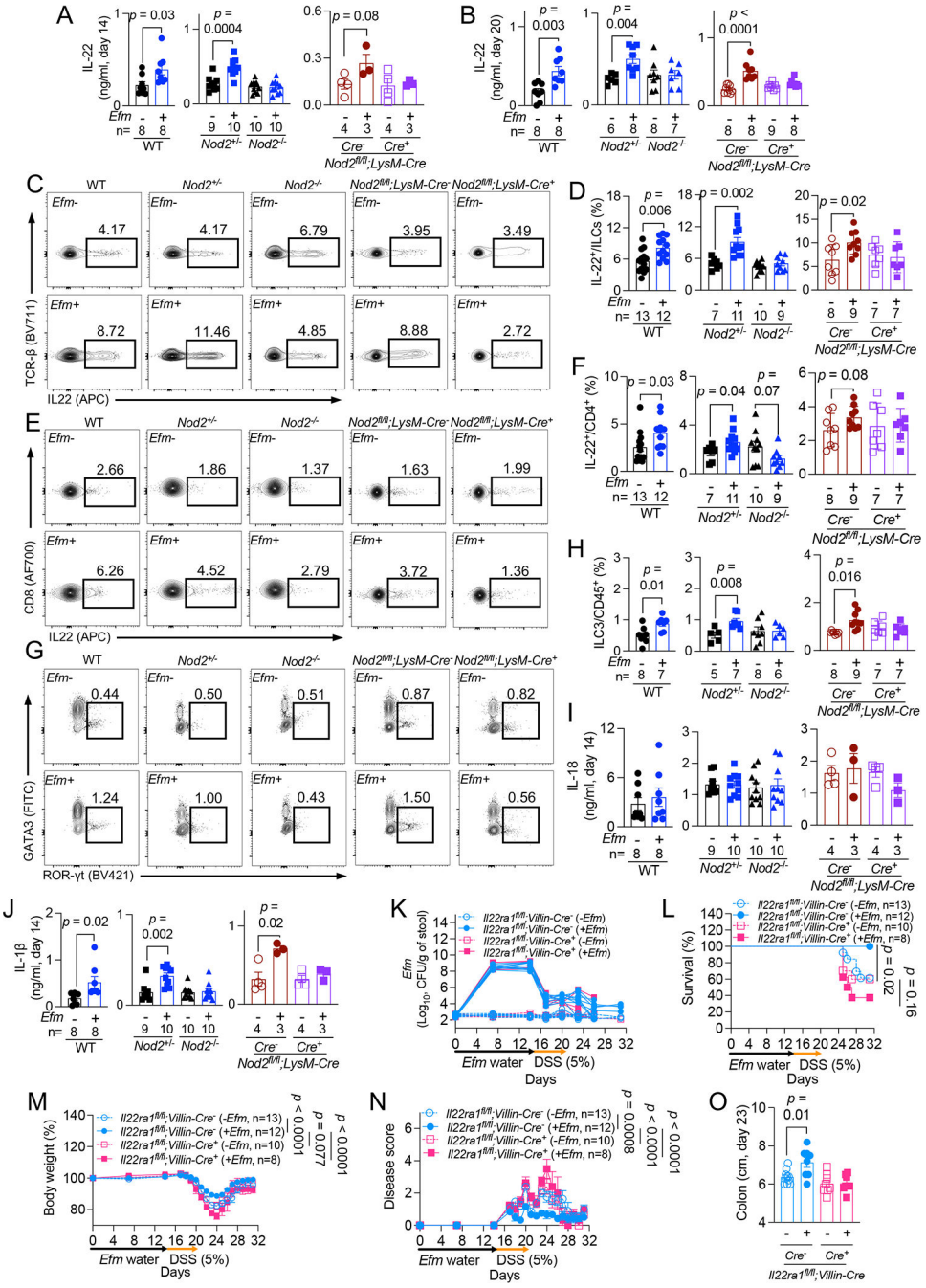

Figure 6. IL-1β induced by *Efm* protective IL-22-producing lymphoid cells.

A and B) Quantification of IL-22 on days 14 (A) and 20 (B) in gut explants from WT, *Nod2*$^{+/-}$, *Nod2*$^{-/-}$, and *Nod2*$^{fl/fl}$*;LysM-Cre*$^{-}$ and *Cre*$^{+}$ mice ± *Efm* inoculation. **C-F)** Representative flow cytometry plots and quantification of proportion of colonic IL-22^{+} innate lymphoid cells (ILCs) (C and D) and CD4^{+} T cells (E and F) in indicated mice ± *Efm* inoculation. **G and H)** Representative flow cytometry plots and quantification of group 3 ILCs (ILC3s) from mice in C-F. **I and J)** Quantification of IL-18 (I) and IL-1β (J) in gut explants from A. **K-O)** DSS treatment of *Il22ra1*$^{fl/fl}$*;Villin-Cre*$^{-}$ and *Cre*$^{+}$ mice following

administration of *Efm* or control examined for *Efm* burden in the stool (K), survival (L), changes in body weight (M), disease score (N), and colon length on day 23 (O). Data points in A, B, D, F, H-J, and O and lines in K represent individual mice. Data points in M and N represent mean ± SEM. Bars represent mean ± SEM and at least two independent experiments were performed. Indicated *p* values by unpaired *t* test, two-tailed in A, B, D, F, H, J, and O, log-rank Mantel-Cox test in L, and two-way ANOVA test in M and N. See also Figures S5 and S6.

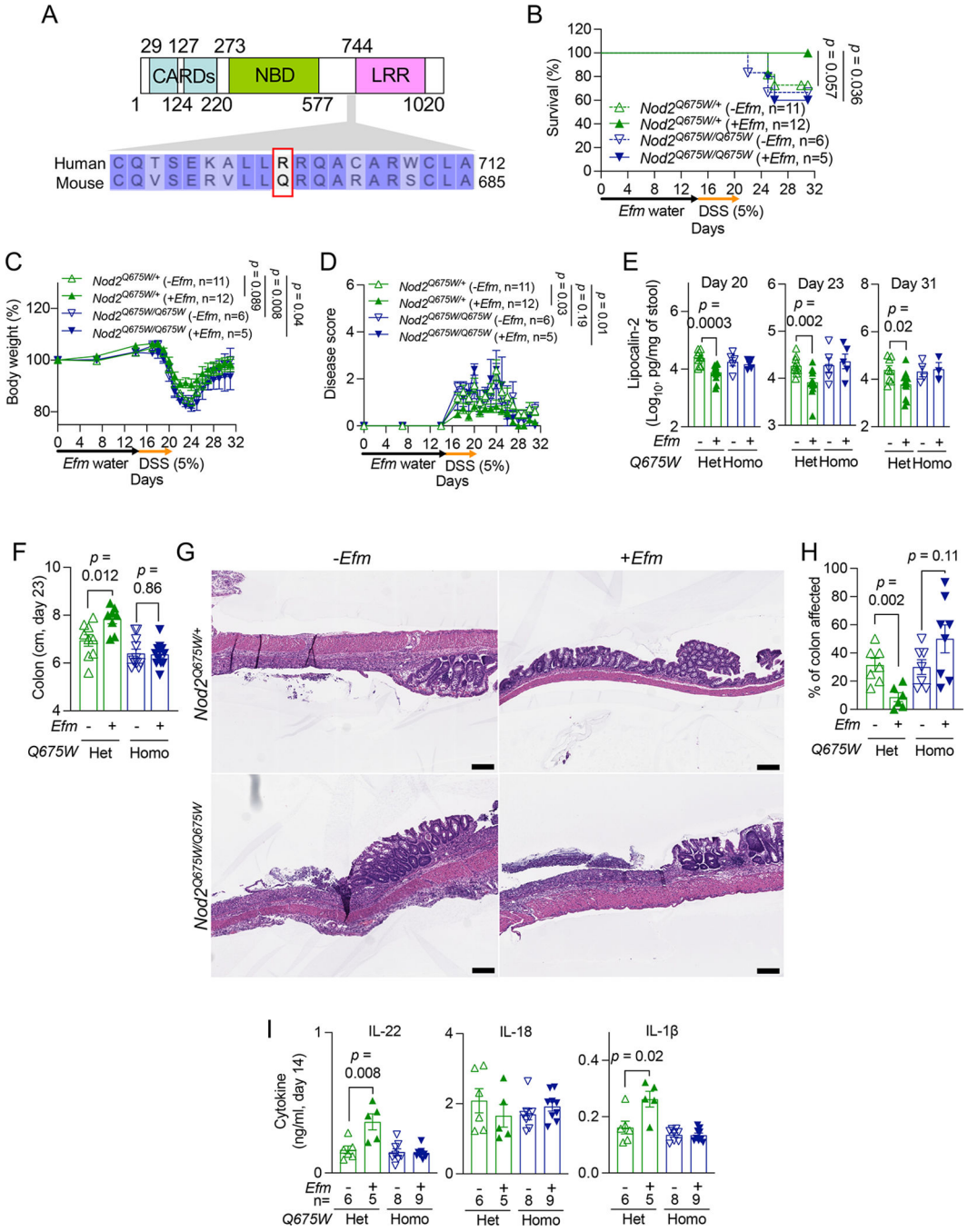

Figure 7. NOD2 Q675W impairs *Efm*-mediated protection.

A) NOD2 protein region targeted by mutagenesis. Arginine at position 702 in human NOD2 and the corresponding glutamine at position 675 in mouse NOD2 are indicated in the red box. Numbers refer to human amino acid positions. **B-F)** DSS-treated *Nod2*$^{Q675W/+}$ and *Nod2*$^{Q675W/Q675W}$ mice ± *Efm* inoculation were examined for survival (B), changes in body weight (C), disease score (D), fecal LCN2 (E), and colon length (F) on day 23. **G and H)** Representative images of H&E-stained sections of the colon (G) and quantification of the proportion of colon affected (H). **I)** Quantification of IL-22 (left), IL-18 (middle), and

IL-1β (right) on day 14 in gut explants from *Nod2*$^{Q675W/+}$ and *Nod2*$^{Q675W/Q675W}$ mice ± *Efm* inoculation. Bars, 200 μM. Data points in E, F, H, and I represent individual mice. Data points in C and D represent mean ± SEM. Bars represent mean ± SEM from at least two independent experiments. CARD, caspase recruitment domain; NBD, nucleotide-binding domain; LRR, leucine-rich repeat domain; Het, heterozygotes; Homo, homozygotes. Indicated *p* values by log-rank Mantel-Cox test in B, two-way ANOVA test in C and D, and unpaired *t* test, two-tailed in E, F, H, and I. See also Figures S7 and Table S4.

KEY RESOURCES TABLE

REAGENT or RESOURCE	SOURCE	IDENTIFIER
Antibodies		
Rat anti-Human Reg1A antibody	R&D Systems	Cat#: MAB4937; RRID: AB_2102139; Clone: 431202
Mouse anti-Human Reg3A antibody	R&D Systems	Cat#: 62257S; RRID: AB_1964697; Clone: 512124
Rabbit anti-REG3G antibody	Abcam	Cat#: ab233480
Rabbit anti-REG4 antibody	Abcam	Cat#: ab255820; Clone: EPR22810-327
Rabbit anti-SagA antibody	Dr. Hang (Scripps Research Institutes)[41]	
Mouse anti-IL-22 antibody	R&D Systems	Cat#: MAB782; RRID: AB_2295882; Clone: 142938
Mouse anti-NOD2 antibody	Invitrogen	Cat#: MA1-16611; RRID: AB_568643; Clone: 2D9
Mouse anti-β-Actin antibody	Sigma	Cat#: A5441; RRID: AB_476744; Clone: AC-15
IRDye 680RD Goat anti-Rabbit IgG Secondary Antibody	LI-COR	Cat# 925-68071; RRID: AB_2721181;
IRDye 800CW Goat anti-Mouse IgG Secondary Antibody	LI-COR	Cat#: 925-32210; RRID: AB_2687825;
IRDye 800CW Goat anti-Rat IgG Secondary Antibody	LI-COR	Cat#: 925-32219; RRID: AB_2721932;
PerCP/Cyanine5.5 anti-mouse/human CD11b Antibody	Biolegend	Cat#: 101228; RRID: AB_893232; Clone: M1/70
PerCP/Cyanine5.5 anti-mouse CD11c Antibody	Biolegend	Cat#: 117328; RRID: AB_2129641; Clone: N418
PerCP/Cyanine5.5 anti-mouse Ly-6G/Ly-6C (Gr-1) Antibody	Biolegend	Cat#: 108428; RRID: AB_893558; Clone: RB6-8C5
PerCP/Cyanine5.5 anti-mouse TER-119/Erythroid Cells Antibody	Biolegend	Cat#: 116228; RRID: AB_893636; Clone: TER-119
PerCP/Cyanine5.5 anti-mouse NK-1.1 Antibody	Biolegend	Cat#: 108728; RRID: AB_2132705; Clone: PK136
PE anti-T-bet Antibody	Biolegend	Cat#: 644810; RRID: AB_2200542; Clone: 4B10
PE- Cyanine7 anti-mouse/human CD44 antibody	Biolegend	Cat#: 103030; RRID: AB_830787; Clone: IM7
APC/Cyanine7 anti-mouse CD4 Antibody	Biolegend	Cat#: 100414; RRID: AB_312699; Clone: GK1.5
Brilliant Violet 570 anti-mouse CD62L Antibody	Biolegend	Cat#: 104433; RRID: AB_10900262; Clone: MEL-14
Brilliant Violet 605 anti-mouse CD127 (IL-7Ra) Antibody	Biolegend	Cat#: 135041; RRID: AB_2572047; Clone: A7R34
Brilliant Violet 650 anti-mouse NK-1.1 Antibody	Biolegend	Cat#: 108736; RRID: AB_2563159; Clone: PK136
Alexa Fluor 700 anti-mouse CD8a Antibody	Biolegend	Cat#: 100730; RRID: AB_493703; Clone: 53-6.7
Brilliant Violet 711 anti-mouse TCR β chain Antibody	Biolegend	Cat#: 109243; RRID: AB_2629564; Clone: H57-597
PerCP/Cyanine5.5 anti-mouse CD19	eBioscience	Cat#: 45-0193-82; RRID: AB_1106999; Clone: 1D3

REAGENT or RESOURCE	SOURCE	IDENTIFIER
PE anti-mouse IL-22 Antibody	eBioscience	Cat#: 12-7221-82; RRID: AB_10597428; Clone: 1H8PWSR
APC anti-mouse FOXP3 Antibody	eBioscience	Cat#: 17-5773-82; RRID: AB_469457; Clone: FJK-16s
PE-CF594 anti-mouse γδ T-Cell Receptor Antibody	BD Bioscience	Cat#: 563532; RRID: AB_2661844; Clone: GL3
BUV395 anti-mouse CD45 Antibody	BD Bioscience	Cat#: 564279; RRID: AB_2651134; Clone: 30-F11
BV421 anti-mouse RORgt Antibody	BD Bioscience	Cat#: 562894; RRID: AB_2687545; Clone: Q31-378
BV421 anti-mouse IL-10 Antibody	BD Bioscience	Cat#: 566295; RRID: AB_2739668; Clone: JES5-16E3
Alexa Fluor 488 anti-mouse GATA3 Antibody	BD Bioscience	Cat#: 560163; RRID: AB_1645302; Clone: L50-823
Bacterial strains		
Enterococcus faecalis OG1RF	Dr. Hang (Scripps Research Institutes), originally acquired from ATCC 47077.	N/A
Enterococcus faecium Com15	Dr. Hang (Scripps Research Institutes), originally acquired Dr. Gilmore (Harvard Medical School).	N/A
Salmonella Typhimurium SL1344	Gift from Dr. Littman (NYU)	N/A
Lactococcus lactis thyA auxotroph	Dr. Hang (Scripps Research Institutes)[50], generated in collaboration with Rise Therapeutics	N/A
Lactococcus lactis thyA expressing wild-type SagA	Dr. Hang (Scripps Research Institutes)[50], generated in collaboration with Rise Therapeutics	N/A
Lactococcus lactis thyA expressing catalytic mutant SagA	Dr. Hang (Scripps Research Institutes)[50], generated in collaboration with Rise Therapeutics	N/A
Chemicals, Peptides, and Recombinant Proteins		
Bacto brain heart infusion	BD	Cat#: 237500
Sabouraud dextrose broth	Millipore	Cat#: S3306
Nutrient Broth	Millipore	Cat#: 70122
BsaHI	NEB	Cat#: R0556S
Dulbecco's Modified Eagle's Medium	Corning	Cat#: 10-017-CV
Fetal bovine serum	Peak Serum	Cat#: PS-FB2
Penicillin-Streptomycin Solution	Corning	Cat#: 30-002-CI
Normicin	InvivoGen	Cat#: ant-nr
Zeocin	InvivoGen	Cat#: ant-zn
Blastocidin	InvivoGen	Cat#: ant-bl
Trypsin-EDTA	Gibco	Cat#: 25200056
M17 Broth	BD	Cat#: 218561
M17 Agar	BD	Cat#: 218571

REAGENT or RESOURCE	SOURCE	IDENTIFIER
Bile esculin azide agar	Millipore	Cat#: 06105
HiCrome Enterococcus faecium Agar Base	HIMEDIA	Cat#: M1580
Enterococcus faecium Selective Supplement	HIMEDIA	Cat#: FD226
Lactose	Sigma-Aldrich	Cat#: 17814
Thymidine	Sigma-Aldrich	Cat#: T9250
Phosphate-buffer saline	Corning	Cat#: 21040CV
Triton X-100	Sigma-Aldrich	Cat#: T8787
Glycerol	Sigma-Aldrich	Cat#: G5516
Halt Protease and Phosphatase Inhibitor Cocktail	Thermo Fisher	Cat#: 78440
Bolt 4-12% Bis-Tris Plus Gels	Invitrogen	Cat#: NW04120BOX
Intercept (TBS) Blocking Buffer	LI-COR	Cat#: 927-60003
Trypticase soy agar with 5% sheep blood	Henry Schein	Cat#: 9873908
HEK-Blue detection medium	InvivoGen	Cat#: hb-det2
Dextran sulfate sodium	TdB Consultancy	Cat#: DB001
Ampicillin	Amercian Bioanalytical	Cat#: 69-52-3
Streptomycin	Sigma-Aldrich	Cat#: S6501
Low melting point agar	Promega	Cat#: V2111
10% Formalin	Thermo Fisher	Cat#: SF99-4
Roswell Park Memorial Institute 1640 Medium	Gibco	Cat#: 61870127
L-glutamine	Corning	Cat#: 25-005-CI
HEPES	Corning	Cat#: 25-060-CI
Minimum Essential Medium Nonessential Amino Acids	Corning	Cat#: 25-025-CI
Sodium pyruvate	Corning	Cat#: 25-000-CI
β-mercaptoethanol	Gibco	Cat#: 21985023
Hank’s Balanced Salt Solution	Gibco	Cat#: 14175103
DL-dithiothreitol	Sigma Aldrich	Cat#: D0632
Collagenase	Sigma Aldrich	Cat#: C2139
Deoxyribonuclease I	Sigma Aldrich	Cat#: DN25
Percoll	Sigma-Aldrich	Cat#: P1644
Cell Stimulation Cocktail (plus protein transport inhibitors)	eBioscience	Cat#: 00-4975-93
Bovine Serum Albumin	Thermo Fisher	Cat#: BP1600-100
Fixation Buffer	Biolegend	Cat#: 420801
Intracellular Staining Permeabilization Wash Buffer	Biolegend	Cat#: 421002
Foxp3 / Transcription Factor Staining Buffer Set	Thermo Fisher	Cat#: 00-5523-00
Zombie UV Fixable Viability Kit	Biolegend	Cat#: 423108
Critical commercial assays		
10 ml syringe	BD	Cat#: 302995
Gauze pad	4MD Medical	Cat#: PROP157025
Millex-GS Syringe Filter Unit, 0.22 μm	Millipore	Cat#: SLGL0250S

REAGENT or RESOURCE	SOURCE	IDENTIFIER
Nalgene Rapid-Flow Sterile Disposable Filter Units with PES Membranes	Thermo Fisher	Cat#: 567-0020
Human Reg3A DuoSet ELISA	R&D systems	Cat#: DY5940-05
Mouse Lipocalin-2/NGAL DuoSet ELISA	R&D systems	Cat#: DY1857-05
Mouse IL-22 DuoSet ELISA	R&D systems	Cat#: DY582-05
Mouse IL-18 DuoSet ELISA	R&D systems	Cat#: DY7625-05
Mouse IL-1 beta/IL-1 F2 DuoSet ELISA	R&D systems	Cat#: DY401-05
DNeasy PowerSoil Pro Kit	Qiagen	Cat#: 47016
MagMAX DNA Multi-Sample Ultra 2.0 kit	Thermo Fisher	Cat#: A36570
RNeasy Mini Kit	Qiagen	Cat#: 74106
RNase-Free DNase Set	Qiagen	Cat#: 79256
70 μm nylon mesh	ELKO Filtering	Cat#: 03-70/33
High-Capacity cDNA Reverse Transcription Kit	Thermo Fisher	Cat#: 4368814
LightCycler 480 SYBR Green I Master	Roche	Cat#: 04707516001
TOPO TA Cloning Kit	Invitrogen	Cat#: 450002
Experimental Models: Organisms/Strains		
Mouse: *Nod2*$^{-/-}$	Jackson Laboratory	Cat#: 005763
Mouse *Nod2*$^{fl/fl}$	Dr. Keestra-Gounder (University of Colorado Anschutz Medical Campus)	N/A
Mouse: *Il22ra1*$^{fl/fl}$	Dr. Sergei Koralov (New York University Grossman school of medicine), originally acquired from Jackson Laboratory (Cat#: 031003)	N/A
Mouse: *LysM-Cre*	Jackson Laboratory	Cat#: 004781
Mouse: *Villin-Cre*	Jackson Laboratory	Cat#: 004586
Mouse: *Il1r1*	Jackson Laboratory	Cat#: 003245
Mouse *Nlrp3*	Jackson Laboratory	Cat#: 021302
Mouse: *Nod2*$^{Q675W/Q675W}$	This study	N/A
Cell line: HEK-Blue Null2	InvivoGen	Cat#: hkb-hnod2
Cell line: HEK-Blue NOD2	InvivoGen	Cat#: hkb-null2
Deposited data		
16S rRNA sequencing data related to Figure 2	This study	BioProject: PRJNA915760
Whole genome sequencing data related to Figure S1	This study	BioProject: PRJNA978059
16S rRNA sequencing data related to Figure S6	This study	BioProject: PRJNA977252
Software and Algorithms		
Prism 9	GraphPad Software	https://www.graphpad.com/scientific-software/prism/
FlowJo	BD	https://www.flowjo.com
NCBI Gene and Protein Data Base	NCBI	http://www.ncbi.nlm.nih.gov
Nucleotide blast	NCBI	https://blast.ncbi.nlm.nih.gov/Blast.cgi
Blastx	NCBI	https://blast.ncbi.nlm.nih.gov/Blast.cgi

REAGENT or RESOURCE	SOURCE	IDENTIFIER
Fiji/ImageJ	NIH	https://fiji.sc